Available online at www.sciencedirect.com
SCIENCE DIRECT®
Catalysis Today 90 (2004) 231–244
CATALYSIS TODAY
www.elsevier.com/locate/cattod

# The relationship of structural defect–redox property–catalytic performance of perovskites and their related compounds for CO and $NO_x$ removal

Hongxing Dai [a,*], Hong He [a,†], Peiheng Li [a], Lizhen Gao [b], Chak-Tong Au [c]

[a] *Department of Applied Chemistry, College of Environmental and Energy Engineering, Beijing University of Technology, Beijing 100022, PR China*
[b] *Department of Applied Chemistry, Shenzhen University, Shenzhen 518060, PR China*
[c] *Department of Chemistry, Hong Kong Baptist University, Kowloon Tong, Hong Kong*

**Abstract**

Perovskite-type oxides $La_{1-x}A'_xCo_{1-y}Bi_yO_{3-\delta}$ ($A'_x = Ba_{0.2}$, $Sr_{0.4}$; $y = 0$, 0.2) and $La_{1-x}Sr_xMO_{3-\delta}$ ($M = Co_{0.77}Bi_{0.20}Pd_{0.03}$, $x = 0$, 0.2, 0.4) and perovskite-like oxides $La_{1.867}Th_{0.100}CuO_{4-\delta}$, $Nd_{2-x}A'_xCuO_{4-\delta}$ ($A'_x = Ba_{0.4}$, $Ce_{0.2}$), and $YBa_2Cu_3O_{7-\delta}$ have been investigated as catalysts for CO oxidation, NO removal, and $N_2O$ decomposition, respectively. X-ray diffraction results revealed that (i) all of these materials were single phase, and (ii) the crystal structures of $La_{1-x}A'_xCo_{1-y}Bi_yO_{3-\delta}$, $La_{1-x}Sr_xMO_{3-\delta}$, $La_{1.867}Th_{0.100}CuO_{4-\delta}$, $Nd_{2-x}A'_xCuO_{4-\delta}$, and $YBa_2Cu_3O_{7-\delta}$ were cubic, orthorhombic, tetragonal (T structure), tetragonal (T′ structure), and orthorhombic, respectively. The results of chemical analysis indicated that (i) there were $Co^{4+}/Co^{3+}$ ions in $La_{1-x}A'_xCoO_{3-\delta}$ ($A'_x = Ba_{0.2}$, $Sr_{0.4}$), $Co^{2+}/Co^{3+}$ and $Bi^{5+}/Bi^{3+}$ ions in $La_{1-x}A'_xCo_{0.8}Bi_{0.2}O_{3-\delta}$ ($A'_x = Ba_{0.2}$, $Sr_{0.4}$) and $La_{1-x}Sr_xMO_{3-\delta}$, $Cu^{2+}/Cu^{3+}$ ions in $La_{1.867}Th_{0.100}CuO_{4-\delta}$, $Nd_2CuO_{4-\delta}$, $Nd_{1.6}Ba_{0.4}CuO_{4-\delta}$, and $YBa_2Cu_3O_{7-\delta}$; and (ii) after pretreatments in $H_2$ or helium at certain temperature, $Cu^+/Cu^{2+}$ ion couples appeared in these cuprate samples. Oxygen isotope exchange experiments indicated that the lattice oxygen mobility in the Bi-doped catalysts were much higher than that in the Bi-free ones. TPR results showed that lattice oxygen in the former samples could be reduced at temperatures lower than those in the latter samples. In the oxidation of CO, the Bi-incorporated catalysts performed much better than the corresponding Bi-free catalysts, the Sr-substituted perovskites showed higher catalytic activities than the Ba-substituted ones; among $La_{1-x}Sr_xMO_{3-\delta}$, $La_{0.8}Sr_{0.2}MO_{2.90}$ exhibited the best catalytic activity. The improved catalytic performance due to the Sr (or Ba)- and Bi-doping is believed to be associated with the enhancements in oxygen vacancy density and $Co^{n+}/Co^{(n+1)+}$ ($n = 2$, 3) and $Bi^{3+}/Bi^{5+}$ couple redox ability as well as in lattice oxygen mobility. In the elimination of NO over $La_{1-x}Sr_xMO_{3-\delta}$, $La_{0.8}Sr_{0.2}MO_{2.90}$ performed the best. The 300 °C-reduced $La_{1.867}Th_{0.100}CuO_{4-\delta}$ catalyst that possessed dual cationic and anionic defects and $Cu^+/Cu^{2+}$ couple showed higher DeNO activity than the fresh one; the redox action between $Cu^+$ and $Cu^{2+}$ is an essential process for NO decomposition. In the decomposition of $N_2O$, the 800 °C-treated $Nd_{2-x}A'_xCuO_{4-\delta}$ ($A'_x = Ba_{0.4}$, $Ce_{0.2}$) and $YBa_2Cu_3O_{7-\delta}$ samples were superior in catalytic performance to their fresh counterparts; oxygen vacancies were favorable for the formation of the crucial $N_2O_2^{2-}$ intermediate species in $N_2O$ activation, and the redox $Cu^{p+}/Cu^{(p+1)+}$ ($p = 1$ and 2) couples involved in the $N_2O$ decomposition processes. The De$N_2O$ activity over the Ce- or Ba-doped catalyst was much better than that over the undoped catalyst ($Nd_2CuO_{4-\delta}$). This behavior is intimately related to the oxygen nonstoichiometry and copper ion redox properties.

According to the outcome of our experiments, we conclude that there is a strong correlation either between the structural defect (mainly oxygen vacancies) and catalytic activity or between the redox [$Co^{n+}/Co^{(n+1)+}$ ($n = 2$, 3), $Bi^{3+}/Bi^{5+}$, and $Cu^{p+}/Cu^{(p+1)+}$ ($p = 1$ and 2) couples] ability and catalytic performance of these materials for CO and $NO_x$ removal. The generation of oxygen vacancies by A-site replacements favors the activation of $O_2$ and $NO_x$; the modification of B-site ion oxidation states by aliovalent ion substitutions in A- and/or B-sites promotes the redox process of the catalyst. Both actions influence the mobility of lattice oxygen. As a result of the combined effect, one can generate a kind of materials that show good catalytic performance for the elimination of CO and $NO_x$.


*Keywords:* Perovskite oxide catalysts; $^{18}O/^{16}O$ isotopic exchange; Lattice oxygen mobility; Oxidative nonstoichiometry; CO oxidation; NO removal; $N_2O$ decomposition; De$NO_x$

* Corresponding author. Tel.: +86-10-6739-6588; fax: +86-10-6739-1983.
*E-mail addresses:* hxdai@bjpu.edu.cn (H. Dai), hehong@bjpu.edu.cn (H. He).
† Co-corresponding author.

0920-5861/$ – see front matter © 2004 Elsevier B.V. All rights reserved.
doi:10.1016/j.cattod.2004.04.031

## 1. Introduction

In the past years, perovskite-type oxides ($ABO_{3-\delta}$), perovskite-like oxides ($A_2BO_{4-\delta}$), and layered perovskite oxides (e.g. $YBa_2Cu_3O_{7-\delta}$) have been investigated extensively and intensively for the total oxidation of carbon monoxide and hydrocarbons [1,2]. The good catalytic activities of these materials are due to the presence of a large number of structural defects such as cationic and anionic vacancies, among which excessive- or deficient-oxygen stoichiometry is the most common case. Another reason for the good catalytic performance is the strong redox ability derived from the coexistence of at least two kinds of oxidation states of the transition metal ion. Therefore, the amount of nonstoichiometric oxygen and the ability of redox determine the catalytic property of the perovskite. By partial substitution of ions in site A and/or site B, one can regulate the amount of oxygen nonstoichiometry and the valence distribution of the B-site ion. The controllable physicochemical properties of these catalytic materials make them useful models for the study of specific reactions.

The different catalytic properties of $ABO_{3-\delta}$, $A_2BO_{4-\delta}$, and $YBa_2Cu_3O_{7-\delta}$ for the addressed reactions are due to their different structural defects. In the cubic $ABO_3$ lattice (Fig. 1A), the A-site ion is 12-fold coordinated and the B-site ion is sixfold coordinated with $O^{2-}$ ions; the center position is occupied by the A-site ion. Actually, the perovskite structure can be viewed with the B-site ion placed in the center of the octahedron and the A-site ion in the center of the cube. In the lattice of orthorhombic $YBa_2Cu_3O_{7-\delta}$ (Fig. 1B), the $Ba^{2+}$ ions are 10-fold coordinated by $O^{2-}$ ions that form a cuboctahedron with two vertices missing. The $Y^{3+}$ ion is eightfold coordinated by an approximate cube of $O^{2-}$ ions. The bond distances and angles for these polyhedra are typical of the species concerned. The copper ions sit in two crystallographically distinct and chemically dissimilar sites. The Cu(1) site at (0, 0, 0) is surrounded by a square planar oxygen configuration; the Cu(2) site at (0, 0, ca. 0.3555) is five-fold coordinated by a square pyramidal arrangement of oxygens. Compared with the ideal perovskite structure (Fig. 1A), there are two principle sets of oxygen vacancies in $YBa_2Cu_3O_{7-\delta}$ (Fig. 1B): one layer of $O^{2-}$ ions in the (*a*, *b*) plane surrounding the $Y^{3+}$ ion and one line of $O^{2-}$ ions parallel to the *b*-axis. The oxygen vacancy density of $YBa_2Cu_3O_{7-\delta}$ depends mainly upon the conditions adopted for preparation. The site of O(3) at (1/2, 0, 0.3788) was not fully occupied (92.5 ± 3.5% occupancy) [3]. The occupancy of oxygen site O(4) is only 72% in $YBa_2Cu_3O_{7-0.3}$ [4] and those of O(4) and O(3) sites are, respectively, 92 and 95% in $YBa_2Cu_3O_{7-0.19}$ [4]. With

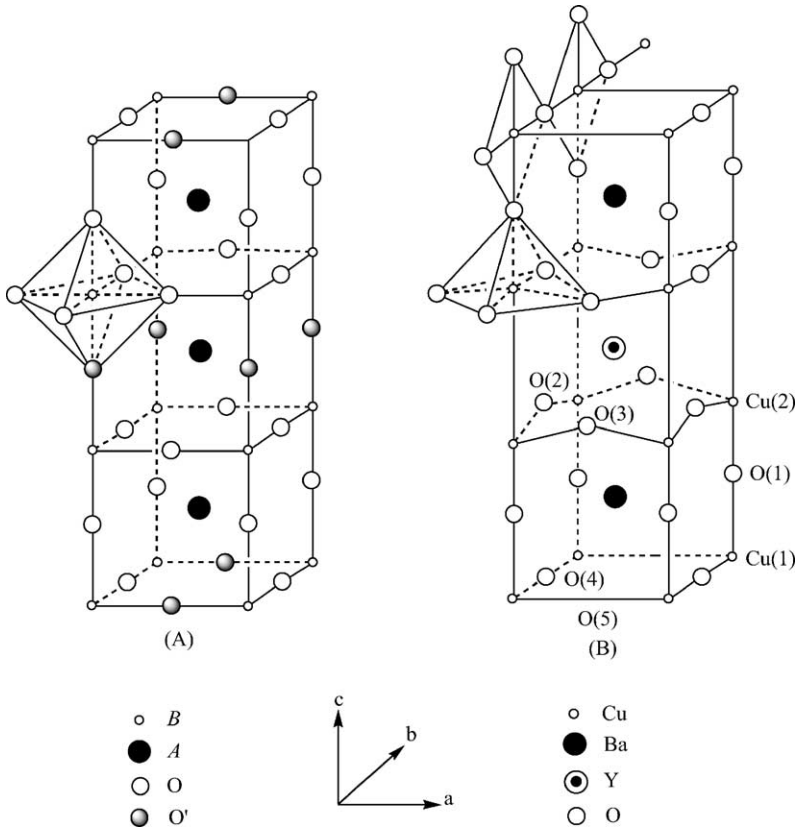


Fig. 1. Schematic structures of (A) perovskite $ABO_3$ and (B) $YBa_2Cu_3O_7$. The atoms O′ are the oxygen atoms of perovskite that do not exist in the structure of $YBa_2Cu_3O_7$. As a consequence of such as elimination, typical chains are formed on the basal plane of the superconductor, and the atoms Cu(2) assume fivefold pyramidal coordination.

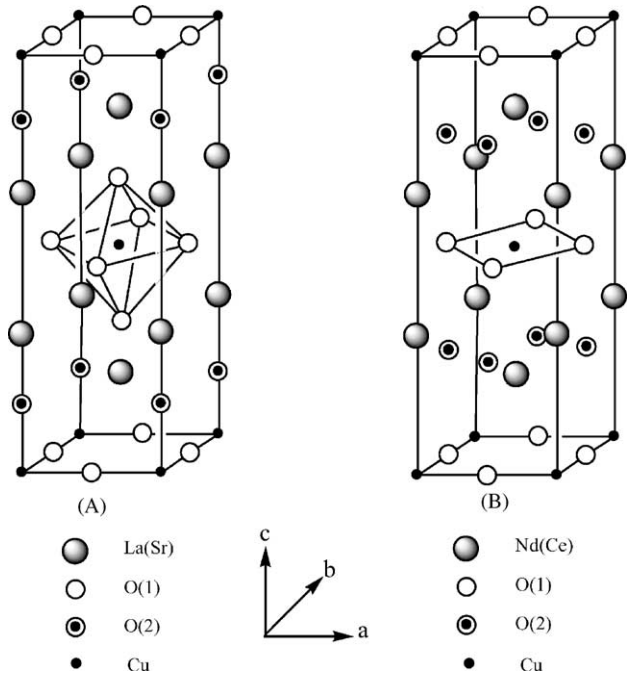


Fig. 2. Schematic structures of (A) $La_{2-x}Sr_xCuO_4$ (T structure) and (B) $Nd_{2-x}Ce_xCuO_4$ (T′ structure).

the rise in temperature, the oxygen atoms removed from the structure are exclusively those located at the O(4) sites [5–7]; further heating at higher temperatures induces more loss of oxygen from the O(4) as well as the O(5) sites at (1/2, 0, 0) until the composition reaches a δ value of 1.0; at this stage, a structural transformation from orthorhombic to tetragonal is expected [6,7]. The $(7-\delta)$ value of the oxygen stoichiometry at such a transformation is always around 6.5. In other words, the orthorhombic phase exists over the range of $0 < \delta \leq 0.5$ and the tetragonal phase over the range of $0.5 \leq \delta < 1.0$. In the tetragonal $La_{2-x}Sr_xCuO_4$ (T structure) and $Nd_{2-x}Ce_xCuO_4$ (T′ structure) lattices, an important structural difference between them is the coordination of the Cu atoms. In the $La_{2-x}Sr_xCuO_4$ structure (Fig. 2A), the Cu atom is located at the corner of a $CuO_6$ octahedron and the La and Sr atoms have ninefold coordinations, whereas in the $Nd_{2-x}Ce_xCuO_4$ structure (Fig. 2B) the Cu is in a $CuO_4$ square and the Nd and Ce atoms have nearly cubic eightfold coordinations. As indicated in Fig. 2, there are two kinds of oxygen atoms [O(1)—apical oxygens—and O(2)]. Oxygen vacancies could be present at both O(1) and O(2) sites [A6]. The fractional occupancy at the O(2) site is slightly lower than that at the O(1) site [8].

Based on the manipulations of chemical characteristics of perovskites, we have recently investigated the effects of substitutions in both cationic sites on the catalytic properties in environmental catalysis [9–13]. In this article, we present the catalytic performance of $La_{1-x}A'_xCo_{1-y}Bi_yO_{3-\delta}$ ($A'_x = Ba_{0.2}$, $Sr_{0.4}$; $y = 0$, 0.2) and $La_{1-x}Sr_xMO_{3-\delta}$ (M = $Co_{0.77}Bi_{0.20}Pd_{0.03}$, $x = 0$–0.4) for CO oxidation and/or NO elimination, $La_{1.867}Th_{0.100}CuO_{4-\delta}$ for NO decomposition, and of $Nd_{2-x}A'_xCuO_{4-\delta}$ ($x = 0$; $A'_x = Ba_{0.4}$, $Ce_{0.2}$) and $YBa_2Cu_3O_{7-\delta}$ for $N_2O$ decomposition and characterized these materials by means of techniques such as XRD (X-ray diffraction), TPR (temperature-programmed reduction), $^{18}O_2$- and CO-pulsing as well as BET and chemical analysis. By comparing the catalytic activities with the characterization results of these materials, we made an attempt to establish correlation(s) between the structural defect and activity and/or between the redox property and activity for the addressed reactions.

## 2. Experimental

### 2.1. Preparation of catalysts

All the catalysts were prepared by adopting the method of citric acid complexing [14]. Stoichiometric amounts of high purity metal nitrates [for $La_{1-x}A'_xCo_{1-y}Bi_yO_{3-\delta}$ ($A'_x = Ba_{0.2}$, $Sr_{0.4}$; $y = 0$, 0.2), $La_{1-x}Sr_xMO_{3-\delta}$ (M = $Co_{0.77}Bi_{0.2}Pd_{0.03}$, $x = 0$, 0.2, 0.4), and $La_{1.867}Th_{0.100}CuO_{4-\delta}$] or oxalates (for $Nd_2CuO_{4-\delta}$, $Nd_{1.6}Ba_{0.4}CuO_{4-\delta}$, $Nd_{1.8}Ce_{0.2}CuO_{4-\delta}$, and $YBa_2Cu_3O_{7-\delta}$) were mixed in aqueous solution. Citric acid equimolar to the metals was added. The solution was then evaporated at 70–80 °C to produce viscous syrup (gel). For the cobaltate samples, the viscous syrups were dried at 120 °C for 8 h and then calcined at 850 °C in air for 18 h; for the cuprate samples, the viscous gels were decomposed abruptly to very fine powders (ca. 10 nm) at 300–400 °C and the powders were then calcined in air at 950 °C for 10–12 h for $La_{1.867}Th_{0.100}CuO_{4-\delta}$ and $YBa_2Cu_3O_{7-\delta}$, and at 1100 °C for 10 h for the Nd-based cuprate samples. The particle size employed was 60–80 (for $La_{1-x}Sr_xMO_{3-\delta}$), 80–100 (for $La_{1-x}A'_xCo_{1-y}Bi_yO_{3-\delta}$), and 100–140 (for $La_{1.867}Th_{0.100}CuO_{4-\delta}$, $Nd_2CuO_{4-\delta}$, $Nd_{1.6}Ba_{0.4}CuO_{4-\delta}$, $Nd_{1.8}Ce_{0.2}CuO_{4-\delta}$, and $YBa_2Cu_3O_{7-\delta}$) meshes. For comparison purposes, we pretreated (i) $La_{1.867}Th_{0.100}CuO_{4-\delta}$ in a mixture of 10% hydrogen-90% helium (flow rate, 20 ml $min^{-1}$) at 300 °C for 3 h, (ii) $YBa_2Cu_3O_{7-\delta}$ in a mixture of 15% hydrogen–85% helium (flow rate, 20 ml $min^{-1}$) at 250 °C for 5 h, and (iii) $Nd_2CuO_{4-\delta}$, $Nd_{1.6}Ba_{0.4}CuO_{4-\delta}$, and $Nd_{1.8}Ce_{0.2}CuO_{4-\delta}$ in helium (flow rate, 20 ml $min^{-1}$) at 800 °C for 1.5 h, respectively.

### 2.2. Determination of catalyst crystal structures and surface areas

The crystal structures of the catalysts were determined by an X-ray diffractometer (D-MAX, Rigaku) operating at 40 kV and 200 mA using Cu Kα radiation and Ni filter. The patterns recorded were referred to the powder diffraction files—1998 ICDD PDF Database for identification. The specific surface areas of the catalysts were measured using $N_2$ adsorption at −196 °C on a Nova 1200 apparatus.

### 2.3. Chemical analysis of Co, Bi and Cu ion oxidation states

The analysis of the oxidation states of $Co^{3+}$ and $Bi^{5+}$ ions in the $La_{0.8}Ba_{0.2}Co_{0.8}Bi_{0.2}O_{3-\delta}$, $La_{0.6}Sr_{0.4}Co_{0.8}Bi_{0.2}O_{3-\delta}$, and $La_{1-x}Sr_xMO_{3-\delta}$ ($x = 0$, 0.2, 0.4) catalysts were carried out using the approach developed by Oku et al. [15]. For the $La_{1-x}A'_xCoO_{3-\delta}$ ($A'_x = Ba_{0.2}$, $Sr_{0.4}$) samples, the $Co^{3+}$ concentration was determined by the iodometric titration method. The contents of copper in different oxidation states in the Cu-containing samples were estimated by means of iodometry according to the procedures adopted by Harris et al. [16]. The experimental errors of the titration approaches were estimated to be ±0.5%.

### 2.4. Determination of catalyst reducibility

The TPR experiments were performed using a Quantasorb surface area analyzer (Quantachrome Corp.) modified with electronic mass flow meters, a programmable furnace, and on-line 13X molecular sieve traps in order to remove the water generated during reduction before thermal conductivity measurements. A flow (40 ml $min^{-1}$) of a 20% $H_2$–80% Ar mixture was employed to reduce the sample (∼15 mg) held within a quartz cell (i.d. = 4 mm) containing a quartz thermowell directly in contact with the sample bed. Reduction profiles were obtained by thermal conductivity measurements of the $H_2$ concentration in the exit stream as the sample temperature was increased from room temperature to 650 °C at 10 °C $min^{-1}$. The thermal conductivity response was calibrated using the complete reduction of CuO powder (Aldrich, 99.995%).

### 2.5. Measurements of catalytic performance

(i) $La_{1-x}A'_xCo_{1-y}Bi_yO_{3-\delta}$ ($A'_x = Ba_{0.2}$, $Sr_{0.4}$; $y = 0$, 0.2). Catalytic evaluation was carried out at atmospheric pressure with 0.2 ml of the catalyst in a fixed-bed quartz micro-reactor (i.d. = 4 mm). The total flow rate of the reactant mixture, (a) 1.75% CO+2.60% $O_2$ + 95.65% He, (b) 1.75% CO + 1.00% $O_2$ + 97.25% He, and (c) 1.75% CO + 0.87% $O_2$ + 97.38% He, was 100 ml $min^{-1}$; the corresponding CO/$O_2$ molar ratio was 0.67/1.00, 1.75/1.00, and 2.01/1.00, respectively, and the space velocity (SV) was 30,000 $h^{-1}$. The inlet and outlet CO concentrations were analyzed on-line by a nondispersive infrared CO/HC gas analyzer (MEXA-324F, Horiba). For the variation of SV, we changed the mass of the catalyst at a fixed flow rate of 100 ml $min^{-1}$.

(ii) $La_{1-x}Sr_xMO_{3-\delta}$. The catalytic activity was evaluated in a quartz tube micro-reactor (i.d. = 10 mm) with gas mixtures simulated to resemble actual automotive exhaust-gas compositions corresponding to an oxidants/reducers stoichiometric factor λ [$\lambda = (2O_2 + NO)/(CO + 9C_3H_6)$] of 1.41, 1.00, and 0.83, respectively; the corresponding feedstock compositions are: (a) 1.40% $O_2$ + 1.61% CO + 500 ppm $C_3H_6$ + 1000 ppm NO, (b) 1.00% $O_2$ + 1.61% CO + 500 ppm $C_3H_6$ + 1000 ppm NO, and (c) 0.80% $O_2$ + 1.61% CO + 500 ppm $C_3H_6$ + 1000 ppm NO, with $N_2$ being the balance gas. The SV was 60,000 $h^{-1}$. The catalyst (500 mg) was packed in the middle of the reactor between two plugs of quartz wool. The reaction temperature was monitored by a thermocouple located at the catalyst bed and regulated from 50 to 500 °C at a rate of 3 °C $min^{-1}$. Before the experiments, the samples were treated in a flow of $N_2$ at 400 °C to scour away surface adspecies. The result of blank run with only quartz wool plugs in the reactor indicated negligible activity below 500 °C. The concentrations of CO, $C_3H_6$, and NO in the reaction system were analyzed on-line by an infrared analyzer (QGS-08B Beijing BAIF), a flame ionization detector (NMH 45), and a Chemiluminescence instrument (Modal 8840, Monitor), respectively.

(iii) $La_{1.867}Th_{0.100}CuO_{4-\delta}$. Catalytic activity evaluation was carried out with 0.3 g of sample packed in a quartz micro-reactor (i.d. = 4 mm). Prior to the test, the sample was treated at 650 °C under a helium flow to eliminate water and carbonates. The decomposition of NO was performed between 200 and 800 °C (heating rate 2 °C $min^{-1}$). The reaction feed was 3000 ppm NO in helium and the SV was 7500 $h^{-1}$. Catalytic activity was measured 0.5 h after performance stabilization. The effluent gases ($N_2$, NO, and $N_2O$) were analyzed on-line by gas chromatography (Shimadzu, GC-8A) and mass spectrometry (HP G1800A). Before evaluating the catalytic activity of the reduced sample, we carried out the $CD_3I$-TPD (temperature-programmed desorption) procedure to eliminate surface hydrogen. After three cycles of $CD_3I$-TPD treatments, we observed no more $CD_3H$. It is an indication that most of the surface hydrogen has been eliminated.

(iv) $Nd_2CuO_{4-\delta}$, $Nd_{1.6}Ba_{0.4}CuO_{4-\delta}$, $Nd_{1.8}Ce_{0.2}CuO_{4-\delta}$, and $YBa_2Cu_3O_{7-\delta}$. Steady-state catalytic activities were measured between 100 and 600 °C at atmospheric pressure, 1 h after performance stabilization over a fixed-bed quartz micro-reactor (i.d. = 4 mm). The sample (100 mg) was pretreated in situ at 800 °C for 1 h in a helium flow before testing. The SV was 60,000 $h^{-1}$ and the feed concentration was 0.6% $N_2O$ with helium being the balance. Gas chromatography and mass spectrometry were used to determine the $N_2O$ decomposition activity.

### 2.6. Isotope oxygen exchanges and carbon monoxide pulsing

Pulse experiments were performed to investigate the reactivity of oxygen species. 0.3 g of the catalyst sample

($La_{0.8}Ba_{0.2}Co_{0.8}Bi_{0.2}O_{3-\delta}$ and $La_{0.6}Sr_{0.4}Co_{0.8}Bi_{0.2}O_{3-\delta}$) was placed in a micro-reactor (i.d. = 4 mm) and was thermally treated in helium (HKO, >99.995%, 20 ml $min^{-1}$) at a desired temperature for 0.5 h. We pulsed $^{18}O_2$ (HKO, 95–98%) onto the sample (helium as carrier gas, 20 ml $min^{-1}$) at various temperatures and monitored the composition of the outlet by means of a mass spectrometer (HP G1800A). The data were taken at the 10th pulse where the reaction reached a steady state. In the CO-pulsing experiments, the sample (which had in turn been treated in helium at 700 °C for 0.5 h and exposed to 100 pulses of $^{18}O_2$ at 500 °C) was exposed to CO pulses (helium as carrier gas, 80 ml $min^{-1}$) at different temperatures and the effluent was analyzed on-line by the mass spectrometer. The pulse size was 50.0 μl (at 25 °C, 1 atm).

## 3. Results

### 3.1. Catalyst structures, compositions, and physical properties

Tables 1 and 2 summarize the crystal structures, compositions, and surface areas of the Co-based catalysts, and the fresh and pretreated Cu-based catalysts, respectively. By comparing the XRD patterns with the ICDD PDF Database data of $LaCoO_3$ (No. 7-0279) and $La_{0.5}Ba_{0.5}CoO_3$ (No. 32-0480), we deduce that (i) $La_{1-x}A'_xCo_{1-y}Bi_yO_{3-\delta}$ ($A'_x$ = $Ba_{0.2}$, $Sr_{0.4}$; $y$ = 0, 0.2) were single-phase perovskites and cubic in structure; and (ii) $La_{1-x}Sr_xMO_{3-\delta}$ ($x$ = 0, 0.2, 0.4) were also single-phase but adopted an orthorhombic perovskite structure. The surface areas are in the range of 6–7 $m^2$ $g^{-1}$. According to the principle of electroneutrality, the amount of oxygen nonstoichiometry ($\delta$) was estimated to be respectively 0.06, 0.13, 0.11, and 0.20 for the La–Ba–Co–O, La–Ba–Co–Bi–O, La–Sr–Co–O, La–Sr–Co–Bi–O perovskite catalysts and −0.07 (at $x$ = 0), 0.10 (at $x$ = 0.2), and 0.19 (at $x$ = 0.4) for the $La_{1-x}Sr_xMO_{3-\delta}$ catalysts. From Table 2, one can observe that all of the Cu-based catalysts were single-phase but the crystal structures were different: (i) tetragonal (T structure as shown in Fig. 2A) for $La_{1.867}Th_{0.100}CuO_{4-\delta}$; (ii) tetragonal (T′ structure as shown in Fig. 2B) for $Nd_2CuO_{4-\delta}$, $Nd_{1.6}Ba_{0.4}CuO_{4-\delta}$, and $Nd_{1.8}Ce_{0.2}CuO_{4-\delta}$; and (iii) orthorhombic for $YBa_2Cu_3O_{7-\delta}$. There were $Cu^{2+}$ and $Cu^{3+}$ in the $La_{1.867}Th_{0.100}CuO_{4-\delta}$, $Nd_2CuO_{4-\delta}$, $Nd_{1.6}Ba_{0.4}CuO_{4-\delta}$, and $YBa_2Cu_3O_{7-\delta}$ samples, and $Cu^+$ and $Cu^{2+}$ in all the partially reduced samples. Furthermore,

Table 1
Crystal structures, surface areas, compositions, oxygen nonstoichiometry, redox ion couples, and activities of the Co-based catalysts

| Catalyst[a] | Crystal phase | Surface area ($m^2$ $g^{-1}$) | $Co^{2+}/Co^{3+}$ (mol%/mol%) | $Co^{3+}/Co^{4+}$ (mol%/mol%) | $Bi^{3+}/Bi^{5+}$ (mol%/mol%) | $\delta$ | $T_{100\%}$[b] (°C) |
|---|---|---|---|---|---|---|---|
| $La_{0.8}Ba_{0.2}CoO_{3-\delta}$ | Cubic | 6.1 | – | 91.7/8.3 | – | 0.06 | 330 |
| $La_{0.8}Ba_{0.2}Co_{0.8}Bi_{0.2}O_{3-\delta}$ | Cubic | 5.6 | 56.1/43.9 | – | 0.8/99.2 | 0.13 | 250 |
| $La_{0.6}Sr_{0.4}CoO_{3-\delta}$ | Cubic | 6.6 | – | 81.4/18.6 | – | 0.11 | 280 |
| $La_{0.6}Sr_{0.4}Co_{0.8}Bi_{0.2}O_{3-\delta}$ | Cubic | 5.8 | 49.8/50.2 | – | 1.4/98.6 | 0.20 | 160 |
| $La_{0.6}Sr_{0.4}MO_{3-\delta}$ | Orthorhombic | 4.5 | 45.6/54.4 | – | 1.2/98.8 | 0.19 | 190 |
| $La_{0.8}Sr_{0.2}MO_{3-\delta}$ | Orthorhombic | 5.2 | 48.8/51.2 | – | 1.0/99.0 | 0.10 | 230 |
| $LaMO_{3-\delta}$ | Orthorhombic | 5.8 | 30.2/69.8 | – | 0.9/99.1 | −0.07 | 290 |

[a] M = $Co_{0.77}Bi_{0.2}Pd_{0.03}$.
[b] $T_{100\%}$ represents the temperature at 100% CO conversion under the conditions of (i) SV = 30,000 $h^{-1}$ and $CO/O_2$ molar ratio = 0.67/1.00 over $La_{1-x}A'_xCo_{1-y}Bi_yO_{3-\delta}$ ($A'_x$ = $Ba_{0.2}$, $Sr_{0.4}$; $y$ = 0, 0.2) and (ii) SV = 60,000 $h^{-1}$ and $\lambda$ = 1.00 over $La_{1-x}Sr_xMO_{3-\delta}$ ($x$ = 0, 0.2, 0.4).

Table 2
Crystal structures, surface areas, compositions, oxygen nonstoichiometry, redox ion couples, and activities of the Cu-based catalysts

| Catalyst[a] | Crystal phase | Surface area ($m^2$ $g^{-1}$) | $Cu^+/Cu^{2+}$ (mol%/mol%) | $Cu^{2+}/Cu^{3+}$ (mol%/mol%) | $\delta$ | Reaction rate[b] ($10^{-4}$ mol $m^{-2}$ $h^{-1}$) |
|---|---|---|---|---|---|---|
| $La_{1.867}Th_{0.100}CuO_{4-\delta}$ | Tetragonal[c] | 3.5 | – | 99.0/1.0 | −0.005 | 10.64 |
| (300 °C-reduced) | | | (4.7/95.3)[d] | – | (0.023) | (17.10) |
| $Nd_2CuO_{4-\delta}$ | Tetragonal[e] | 2.9 | – | 94/6 | −0.03 | 7.60 |
| (800 °C in helium) | | | (10/90) | – | (0.05) | (8.82) |
| $Nd_{1.6}Ba_{0.4}CuO_{4-\delta}$ | Tetragonal[e] | 3.8 | – | 68/32 | 0.04 | 13.30 |
| (800 °C in helium) | | | (25/75) | – | (0.07) | (18.11) |
| $Nd_{1.8}Ce_{0.2}CuO_{4-\delta}$ | Tetragonal[e] | 3.6 | 10/90 | – | −0.05 | 14.44 |
| (800 °C in helium) | | | (36/64) | – | (0.08) | (19.87) |
| $YBa_2Cu_3O_{7-\delta}$ | Orthorhombic | 3.2 | – | 76.1/23.9 | 0.28 | 12.60 |
| (250 °C-reduced) | (Tetragonal) | | (35/65) | – | (0.675) | (18.64) |

[a] Fresh and pretreated (under conditions described in parenthesis) samples.
[b] Reaction rate of NO or $N_2O$ decomposition at 600 °C.
[c] Structure as shown in Fig. 2A.
[d] All the data obtained after the sample was pretreated under conditions described in parenthesis.
[e] Structure as shown in Fig. 2B.

the $Cu^{+}$ concentration in the catalyst increased significantly after reduction or thermal treatment in helium. Considering the titration uncertainty, one can take that the Bi ions were practically pentavalent in the Bi-containing catalysts. The $\delta$ values calculated based on the electroneutrality principle were negative for fresh $La_{1.867}Th_{0.100}CuO_{4-\delta}$, $Nd_2CuO_{4-\delta}$, and $Nd_{1.8}Ce_{0.2}CuO_{4-\delta}$, indicating that the three fresh samples contain excessive oxygen (so-called over-stoichiometric oxygen or oxidative nonstoichiometry); after pretreatment in hydrogen or helium at certain temperatures, however, they became oxygen-deficient (reductive nonstoichiometry) materials. Due to the high calcination temperatures, the surface areas of these samples were generally low ($<4\,m^2\,g^{-1}$).

### 3.2. CO oxidation

Fig. 3 shows the catalytic activities of $La_{0.8}Ba_{0.2}Co_{0.8}Bi_{0.2}O_{2.87}$ and $La_{0.6}Sr_{0.4}Co_{0.8}Bi_{0.2}O_{2.80}$ versus reaction temperature at $30{,}000\,h^{-1}$ and at three different $CO/O_2$ molar ratios. For comparison purposes, the activities of $La_{0.8}Ba_{0.2}CoO_{2.94}$ and $La_{0.6}Sr_{0.4}CoO_{2.89}$ at $CO/O_2$ = 0.67/1.00 are also included. It is observed that with the rise in reaction temperature, CO conversion increased; the extent of increase in activity, however, differed considerably from catalyst to catalyst. Compared to $La_{0.8}Ba_{0.2}CoO_{2.94}$ [$T_{100\%}$ (temperature required for 100% CO conversion) = 330 °C], $La_{0.8}Ba_{0.2}Co_{0.8}Bi_{0.2}O_{2.87}$ ($T_{100\%}$ = 250 °C) exhibited much better catalytic activity under the same conditions (SV = $30{,}000\,h^{-1}$ and $CO/O_2$ = 0.67/1.00). With the oxygen content in the reaction mixture changed from excessive to stoichiometric, CO oxidation activity of the Bi-incorporated catalyst decreased markedly at the same temperature; the $T_{100\%}$ value was 250 °C at $CO/O_2$ = 0.67/1.00, 290 °C at $CO/O_2$ = 1.75/1.00, and 310 °C at $CO/O_2$ = 2.01/1.00 (Fig. 3A). As shown in Fig. 3B, catalytic performance was obviously improved when the substitution amount of Sr for La is higher than that of Ba for La. With the incorporation of Bi into the lattice of $La_{0.6}Sr_{0.4}CoO_{3-\delta}$, the CO oxidation activity increased significantly. Such behavior of dependence on oxygen concentration was also observed over $La_{0.6}Sr_{0.4}Co_{0.8}Bi_{0.2}O_{2.80}$, the value of $T_{100\%}$ was 160 °C at $CO/O_2$ = 0.67/1.00, 180 °C at $CO/O_2$ = 1.75/1.00, and 360 °C at $CO/O_2$ = 2.01/1.00 over the Sr- and Bi-doped catalyst (Fig. 3B). It is apparent that the temperature required for complete CO conversion increases with a drop in $O_2$ content. Compared to the catalysts of supported noble metals (Pt, Pd or Rh), the catalysts of base metal oxides usually exhibit a significant drawback, i.e., there is a rapid decrease in CO conversion at elevated SVs [2]. In order to examine this effect over $La_{0.8}Ba_{0.2}Co_{0.8}Bi_{0.2}O_{2.87}$ and $La_{0.6}Sr_{0.4}Co_{0.8}Bi_{0.2}O_{2.80}$, we tested the catalysts at various SVs and the results are shown in Fig. 4. With the increase in SV from 5000 to $60{,}000\,h^{-1}$ and at $CO/O_2$ = 0.67/1.00, the value of $T_{100\%}$ shifted from 190 to 430 °C for the Ba-substituted catalyst (Fig. 4A) and 130–210 °C for the Sr-substituted catalyst (Fig. 4B). Furthermore, CO conversions augmented at a faster rate at lower SVs. We also observed similar scenarios in the cases of $CO/O_2$ = 1.75/1.00 and 2.01/1.00.

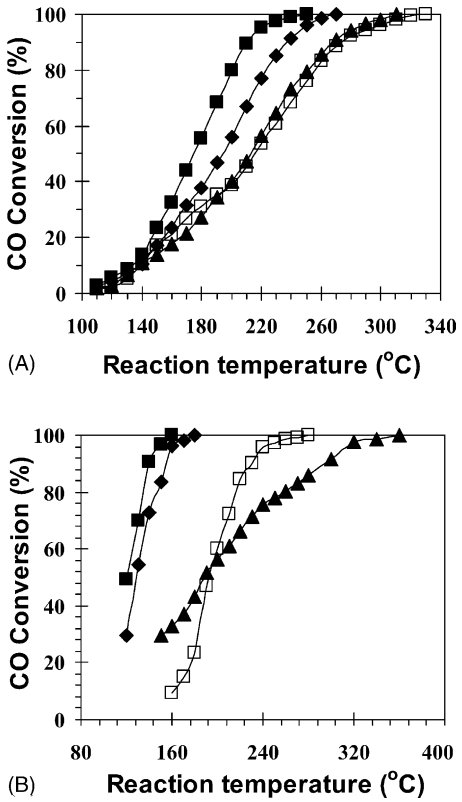


Fig. 3. Catalytic performance of (A) $La_{0.8}Ba_{0.2}CoO_{2.94}$ (□) and $La_{0.8}Ba_{0.2}Co_{0.8}Bi_{0.2}O_{2.87}$ (■, ◆, ▲) and (B) $La_{0.6}Sr_{0.4}CoO_{2.89}$ (□) and $La_{0.6}Sr_{0.4}Co_{0.8}Bi_{0.2}O_{2.80}$ (■, ◆, ▲) as related to reaction temperature at SV = $30{,}000\,h^{-1}$ and $CO/O_2$ molar ratio = 0.67/1.00 (□, ■), 1.75/1.00 (◆), and 2.01/1.00 (▲).

Fig. 5 shows the catalytic performance of $La_{1-x}Sr_xMO_{3-\delta}$ at SV = $60{,}000\,h^{-1}$ and at various stoichiometric factors. From Fig. 5A, one can see that the substitution of Sr for La caused CO conversion to increase significantly and the best catalytic activity was achieved at $x = 0.2$. When $\lambda = 1.41$ and 1.00, the profiles of CO conversion versus temperature were basically the same. After the reaction mixture was switched to reductive atmosphere ($\lambda = 0.83$), however, CO conversion decreased obviously with increasing temperature and CO could not be oxidized completely below 220 °C (Fig. 5B).

Shown in Fig. 6 are the results of $^{18}O_2$-pulsing onto the $La_{0.8}Ba_{0.2}Co_{0.8}Bi_{0.2}O_{2.87}$ and $La_{0.6}Sr_{0.4}Co_{0.8}Bi_{0.2}O_{2.80}$ samples. During the pulsing of $^{18}O_2$, $^{18}O$ infiltrates into the catalyst lattice, driving $^{16}O_2$ and $^{18}O^{16}O$ into the gas phase. It can be seen from Fig. 6A that when the temperature was raised to 200 °C, isotopic exchange (between the $^{18}O$ from the gas phase and the $^{16}O$ in the $La_{0.8}Ba_{0.2}Co_{0.8}Bi_{0.2}O_{2.87}$ lattice) took place. Above 300 °C, the exchange became significant. At 425 °C, the concentration of $^{18}O^{16}O$ was the highest. Further rise in temperature to 500 °C resulted in

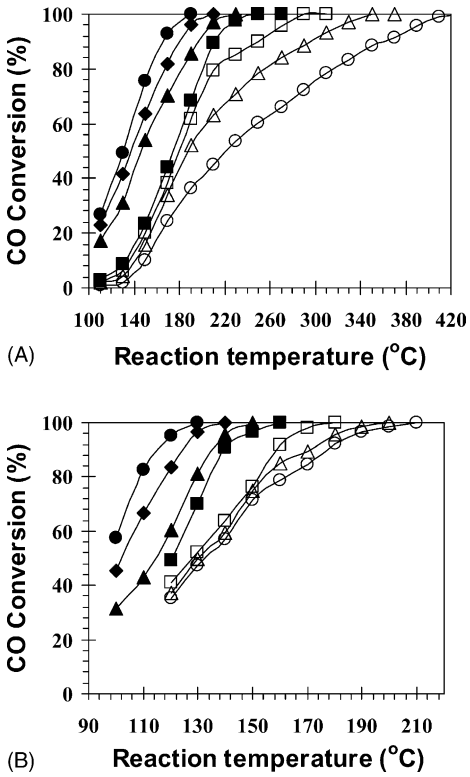


Fig. 4. Catalytic performance of (A) $La_{0.8}Ba_{0.2}Co_{0.8}Bi_{0.2}O_{2.87}$ and (B) $La_{0.6}Sr_{0.4}Co_{0.8}Bi_{0.2}O_{2.80}$ as a function of reaction temperature at $CO/O_2$ molar ratio = 0.67/1.00 and SV=5000 $h^{-1}$ (●), 10,000 $h^{-1}$ (◆), 20,000 $h^{-1}$ (▲), 30,000 $h^{-1}$ (■), 40,000 $h^{-1}$ (□), 50,000 $h^{-1}$ (△), and 60,000 $h^{-1}$ (○).

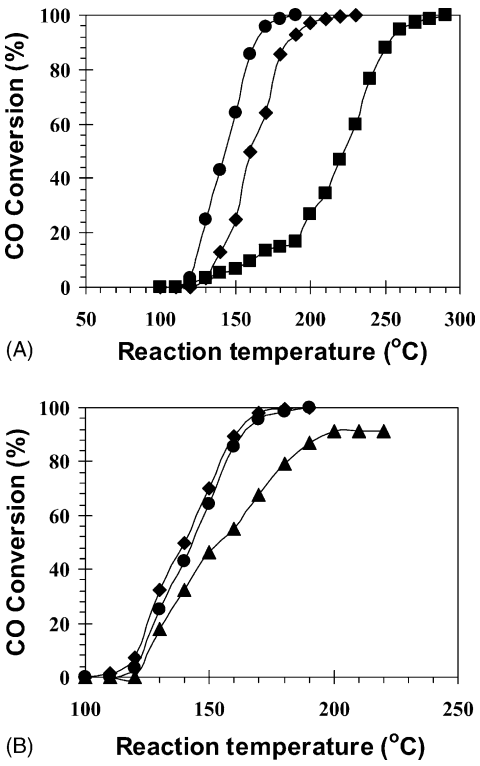


Fig. 5. Catalytic performance of (A) $La_{1-x}Sr_xMO_{3-\delta}$ (M = $Co_{0.77}Bi_{0.2}Pd_{0.03}$; $x = 0$ (■), 0.2 (●), 0.4 (◆)) at SV = 60,000 $h^{-1}$ and $\lambda = 1.00$ and (B) $La_{0.8}Sr_{0.2}MO_{2.90}$ at SV = 60,000 $h^{-1}$, and $\lambda = 1.41$ (◆), 1.00 (●), and 0.83 (▲).

a decrease in $^{18}O^{16}O$ and a considerable increase in $^{16}O_2$ concentration; at 500 °C, the exchange came to a completion. In the case of $La_{0.6}Sr_{0.4}Co_{0.8}Bi_{0.2}O_{2.80}$ (Fig. 6B), isotopic exchange became significant above 250 °C; after reaching the highest level at 350 °C, the $^{18}O^{16}O$ content went down whereas the $^{16}O_2$ concentration went up, and exchange was completed at 500 °C. These results clearly indicate that the lattice oxygens of $La_{0.8}Ba_{0.2}Co_{0.8}Bi_{0.2}O_{2.87}$ and $La_{0.6}Sr_{0.4}Co_{0.8}Bi_{0.2}O_{2.80}$ are mobile above 250 °C and the mobility of lattice oxygen in/on the latter is much higher than that in/on the former. In order to investigate the reactivity of lattice oxygen species, we pulsed CO at various temperatures onto the Bi-doped samples that had been treated in helium at 700 °C for 0.5 h and exposed to 100 pulses of $^{18}O_2$ at 500 °C; the data were obtained at the 10th pulse of CO (Fig. 7). With temperature rise, there was a general increase in CO conversion. Over the $La_{0.8}Ba_{0.2}Co_{0.8}Bi_{0.2}O_{2.87}$ sample (Fig. 7A), between 150 and 250 °C, the selectivity of $C^{16}O_2$ was ca. 75% while that of $C^{18}O^{16}O$ was ca. 30%; the selectivity of $C^{18}O_2$ was below 3%. Over the $La_{0.6}Sr_{0.4}Co_{0.8}Bi_{0.2}O_{2.80}$ sample (Fig. 7B), at 200 °C, the $C^{16}O_2$ selectivity reached the lowest value (56%) whereas the $C^{18}O^{16}O$ selectivity reached the highest value (39%); the $C^{18}O_2$ selectivity was less than 5%. The balance of carbon was found to be within the 99.5–100% range throughout the whole temperature range.

Fig. 8 illustrates the TPR profiles of the Co-based samples. There was a big reduction band at 490 °C for the $La_{0.8}Ba_{0.2}CoO_{2.94}$ sample (Fig. 8a), at 400 °C for the $La_{0.8}Ba_{0.2}Co_{0.8}Bi_{0.2}O_{2.87}$ sample (Fig. 8b), at 440 °C (with a shoulder at 399 °C) for the $La_{0.6}Sr_{0.4}CoO_{2.89}$ sample (Fig. 8c), and at 376 °C (with a shoulder at 480 °C) for the $La_{0.6}Sr_{0.4}Co_{0.8}Bi_{0.2}O_{2.80}$ sample (Fig. 8d). The amount of $H_2$ consumed was 1.88, 3.12, 2.38, 4.81 mmol $H_2$ $g_{cat}^{-1}$, respectively. The bands were generated due to the reduction of Co and/or Bi ions as well as that of oxygen adspecies. Apparently, with the doping of bismuth, the reduction shifted toward lower temperature; i.e., the incorporation of Bi into the perovskite lattice increased the reducibility of the catalyst. In the case of $La_{1-x}Sr_xMO_{3-\delta}$, for the $LaMO_{3.07}$ catalyst, there were reduction bands at 250, 338, and 605 °C (Fig. 8e); the first two bands (0.83 mmol $H_2$ $g_{cat}^{-1}$) were due to the reduction of interstitial oxygen, $Bi^{5+}$ (to $Bi^{3+}$), $Co^{3+}$ (to $Co^{2+}$), and $Pd^{2+}$ (to $Pd^0$), the last band (0.85 mmol $H_2$ $g_{cat}^{-1}$) could be ascribed to the reduction of $Bi^{3+}$ (to $Bi^0$) and $Co^{2+}$ (to $Co^0$). Such an assignment was corroborated by the XRD results (not shown here). There were two partially overlapping reduction bands at 440 and 485 °C for the $La_{0.8}Sr_{0.2}MO_{2.90}$ (Fig. 8f) catalyst and 458 and 485 °C for the $La_{0.6}Sr_{0.4}MO_{2.81}$ (Fig. 8g) catalyst. The

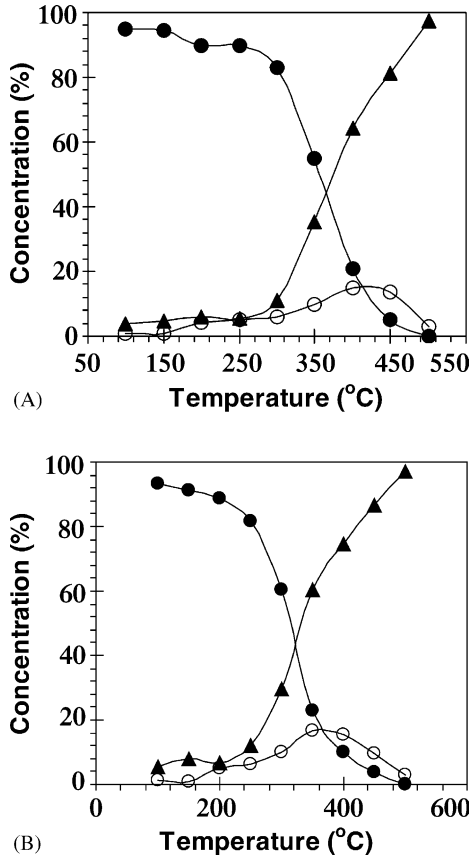


Fig. 6. The distribution of isotopic dioxygen in the $^{18}O/^{16}O$ exchange experiment performed over (A) $La_{0.8}Ba_{0.2}Co_{0.8}Bi_{0.2}O_{2.87}$ and (B) $La_{0.6}Sr_{0.4}Co_{0.8}Bi_{0.2}O_{2.80}$ after treatment in helium at 700 °C for 0.5 h. $^{18}O_2$ (●), $^{16}O_2$ (▲), $^{18}O^{16}O$ (○).

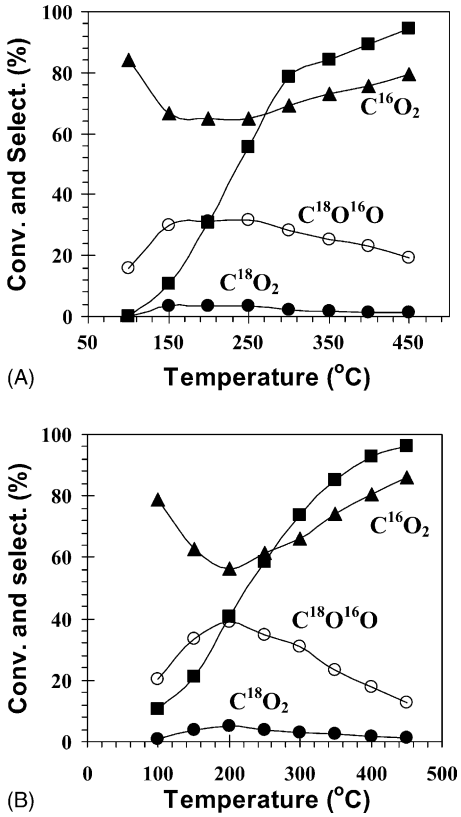


Fig. 7. CO conversion (■) and the distribution of isotopic carbon dioxide at the 10th pulse of CO over (A) $La_{0.8}Ba_{0.2}Co_{0.8}Bi_{0.2}O_{2.87}$ and (B) $La_{0.6}Sr_{0.4}Co_{0.8}Bi_{0.2}O_{2.80}$ (after treatment in helium at 700 °C for 0.5 h and 100 pulses of $^{18}O_2$) at various temperatures.

total amount of $H_2$ consumed was 3.20 and 2.91 mmol $H_2$ $g_{cat}^{-1}$, respectively. Both bands were also due to the reduction of Co, Bi, and Pd ions as well as that of oxygen adspecies.

### 3.3. NO elimination

The catalytic performance in NO elimination over $La_{1-x}Sr_xMO_{3-\delta}$ is shown in Fig. 9. For all the $La_{1-x}Sr_xMO_{3-\delta}$ catalysts, NO conversions first increased and then decreased with temperature rise, the highest NO conversions being 54% at 350 °C when $x = 0$; 97% at 260 °C when $x = 0.2$; 92% at 310 °C when $x = 0.4$ (Fig. 9A). To summarize briefly, the catalytic performance in NO elimination was in the order of $La_{0.8}Sr_{0.2}MO_{2.90}$ > $La_{0.6}Sr_{0.4}MO_{2.81}$ > $LaMO_{3.07}$. From Fig. 9B, one can observe that with the rise in temperature (especially above 350 °C), the selectivity to $N_2$ increased whereas that to $N_2O$ decreased; at 500 °C, 100% $N_2$ selectivity was achieved over $La_{0.8}Sr_{0.2}MO_{2.90}$. Since the catalytic activity in $NO_x$ removal of a catalyst is strongly dependent upon the λ value, we used the best-performing $La_{0.8}Sr_{0.2}MO_{2.90}$ catalyst to examine this effect. The results are presented in Fig. 9C. With a change of λ from 1.00 to 1.41, the maximal NO conversion to $N_2$

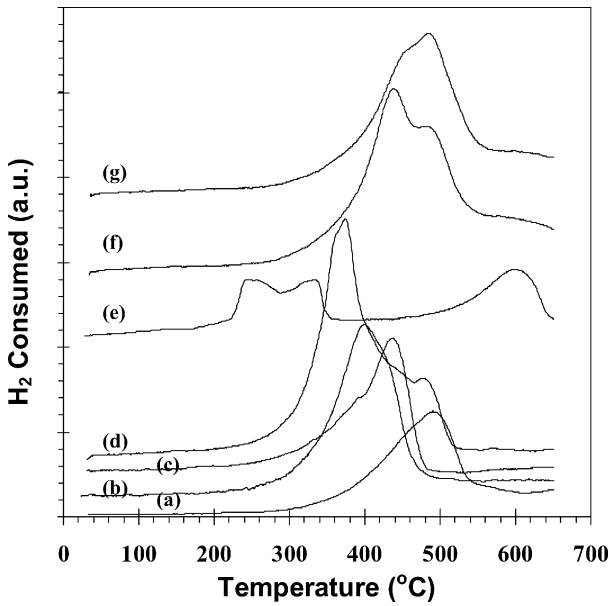


Fig. 8. TPR profiles of (a) $La_{0.8}Ba_{0.2}CoO_{2.94}$, (b) $La_{0.8}Ba_{0.2}Co_{0.8}Bi_{0.2}O_{2.87}$, (c) $La_{0.6}Sr_{0.4}CoO_{2.89}$, (d) $La_{0.6}Sr_{0.4}Co_{0.8}Bi_{0.2}O_{2.80}$, (e) $LaMO_{3.07}$, (f) $La_{0.8}Sr_{0.2}MO_{2.90}$, and (g) $La_{0.6}Sr_{0.4}MO_{2.81}$.

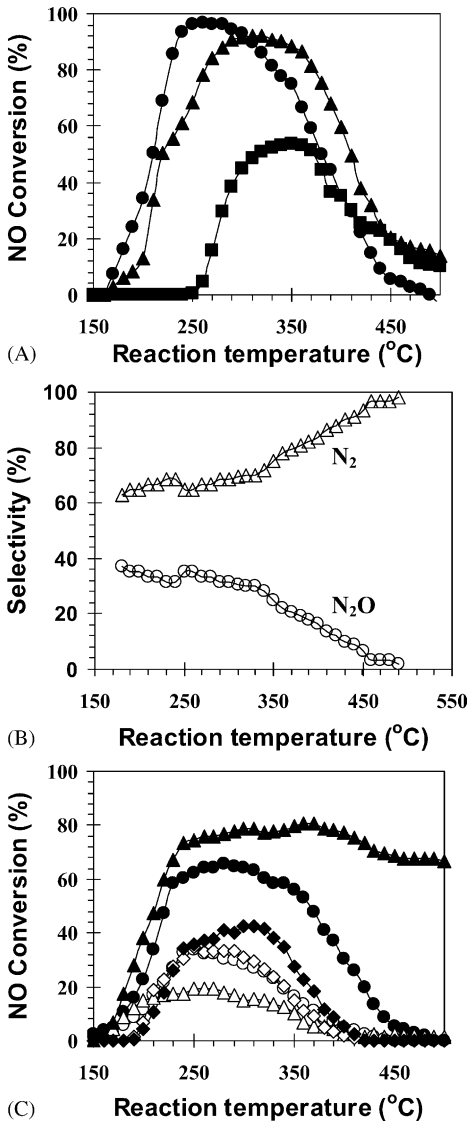


Fig. 9. NO conversion over (A) $La_{1-x}Sr_xMO_{3-\delta}$ (M = $Co_{0.77}Bi_{0.2}Pd_{0.03}$; $x = 0$ (■), 0.2 (●), 0.4 (▲)) at SV = 60,000 $h^{-1}$ and $\lambda = 1.00$, (B) $N_2$ and $N_2O$ selectivities over $La_{0.8}Sr_{0.2}MO_{2.90}$ at SV = 60,000 $h^{-1}$ and $\lambda = 1.00$, and (C) NO conversion over $La_{0.8}Sr_{0.2}MO_{2.90}$ at $SV = 60{,}000\,h^{-1}$ and $\lambda = 1.41$ (◆, ◇), 1.00 (●, ○), and 0.83 (▲, △).

decreased markedly from 64 to 42%; the corresponding NO conversions to $N_2O$ were 32 and 29%. When the λ value was decreased to 0.83, NO conversion to $N_2$ increased while NO conversion to $N_2O$ decreased as expected. It can also be observed that above 220 °C, NO conversion to $N_2$ was much higher than those of the other two cases, and above 450 °C NO conversion to $N_2$ stayed at ca. 67% rather than decreasing to zero as in the cases of $\lambda = 1.00$ and 1.41 (Fig. 9C).

Fig. 10 shows the conversion of NO to $N_2$ and $N_2O$ as a function of temperature over the fresh and 300 °C-reduced $La_{1.867}Th_{0.100}CuO_{4-\delta}$ catalysts. With the rise in temperature, NO conversion to $N_2$, and NO conversion to $N_2O$ first increased and then decreased. Within the temperature range,

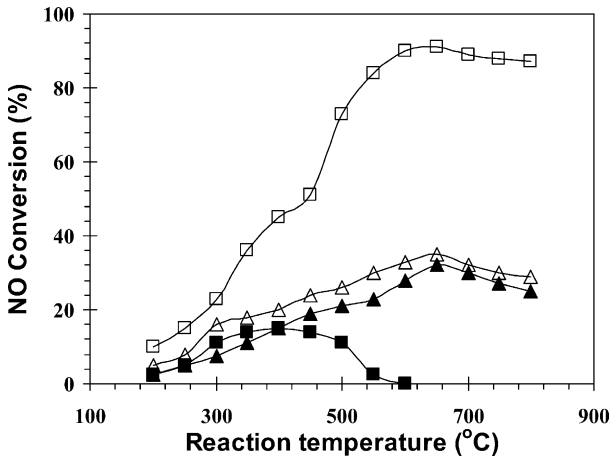


Fig. 10. NO conversion to $N_2$ (△, □) and $N_2O$ (▲, ■) vs. reaction temperature over fresh (△, ▲) and 300 °C-reduced (□, ■) $La_{1.867}Th_{0.100}CuO_{4-\delta}$.

the performance of the reduced sample was much better than that of the fresh one. At 650 °C, we obtained 91% NO conversion (to $N_2$) over the former, and 35% NO conversion (to $N_2$) over the latter.

### 3.4. $N_2O$ decomposition

Shown in Fig. 11 are the $N_2O$ decomposition activities as a function of reaction temperature over the $Nd_2CuO_{4.03}$, $Nd_{1.8}Ce_{0.2}CuO_{4.05}$, and $Nd_{1.6}Ba_{0.4}CuO_{3.96}$ catalysts. The conversion of $N_2O$ over these catalytic materials declined in the order of $Nd_{1.8}Ce_{0.2}CuO_{4.05} > Nd_{1.6}Ba_{0.4}CuO_{3.96} > Nd_2CuO_{4.03}$ when the temperatures were below 400 °C. Above 400 °C, the trend changed to $Nd_{1.6}Ba_{0.4}CuO_{3.96} > Nd_{1.8}Ce_{0.2}CuO_{4.05} > Nd_2CuO_{4.03}$. Fig. 12 shows the $N_2O$ decomposition activities over the fresh and 250 °C-reduced $YBa_2Cu_3O_{7-\delta}$ samples. With the rise in reaction tem-

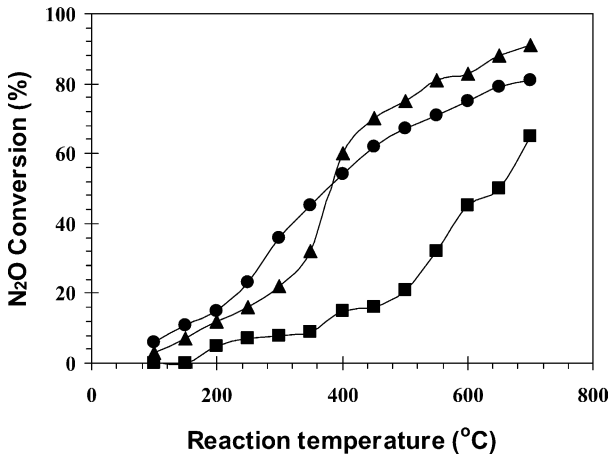


Fig. 11. Steady-state conversion-temperature plots of $N_2O$ decomposition over $Nd_2CuO_{4-\delta}$ (■), $Nd_{1.6}Ba_{0.4}CuO_{4-\delta}$ (▲), and $Nd_{1.8}Ce_{0.2}CuO_{4-\delta}$ (●).

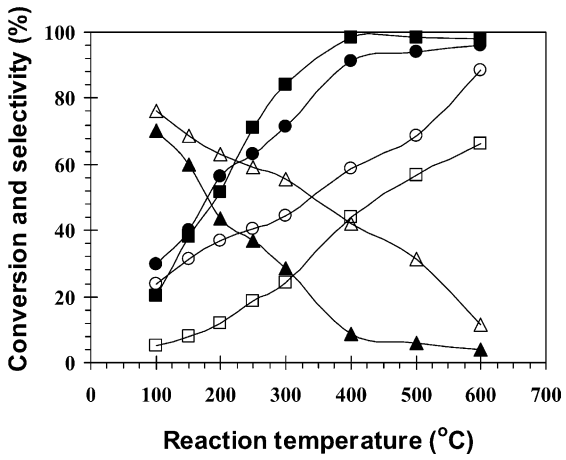


Fig. 12. Catalytic performance of fresh (□, ○, △) and 250 °C-reduced $YBa_2Cu_3O_{7-\delta}$ (■, ●, ▲) as a function of reaction temperature for $N_2O$ decomposition. (□, ■) $N_2O$ conversion, (○, ●) $N_2$ selectivity, and (△, ▲) NO selectivity.

perature, $N_2O$ conversion and $N_2$ selectivity increased rapidly and reached 98 and 91%, respectively, at 400 °C, and the corresponding NO selectivity was 9% over the 250 °C-reduced catalyst; but over the fresh catalyst, $N_2O$ conversion and $N_2$ selectivity increased and NO selectivity decreased in a relatively slow manner. Obviously, the $N_2O$ decomposition activity over the reduced $YBa_2Cu_3O_{7-\delta}$ is higher that that over the fresh one.

## 4. Discussion

### 4.1. Structural defect, redox ion couple, and catalytic activity in CO oxidation

Among the series of A-substituted $LaCoO_3$, Sr-substitution for La has been studied most extensively and intensively [2]. Due to the similarity in chemical properties, Ba-substitution for La and Sr-substitution for La are expected to induce similar effects: the generation of oxygen vacancies and hypervalent cobalt ions ($Co^{4+}$). The positive value of $\delta$ and the presence of $Co^{4+}$ ions in $La_{0.8}Ba_{0.2}CoO_{3-\delta}$ and $La_{0.6}Sr_{0.4}CoO_{3-\delta}$ confirmed such a deduction. Considering that $Bi^{5+}$ is closer in size to Co ions (<0.8 Å), and $Bi^{3+}$ to $La^{3+}$ and $Ba^{2+}$ (>1 Å), and together with the estimation of tolerance factor [2], $Bi^{3+}$ should dwell at the A-sites while $Bi^{5+}$ at the B-sites of $ABO_3$. Such a notion has been substantiated in the investigations of the $K_{1-x}Bi_xBiO_{3-\delta}$ and Ba–Bi–Fe–O perovskite structures [17–20]. It is unusual to have both A- and B-sites occupied by the same element. The result of chemical analysis for Bi oxidation state indicated that the Bi ions in $La_{0.8}Ba_{0.2}Co_{0.8}Bi_{0.2}O_{2.87}$ and $La_{0.6}Sr_{0.4}Co_{0.8}Bi_{0.2}O_{2.80}$ were pentavalent. The incorporation of $Bi^{5+}$ ions into the B-sites enlarges the $La_{0.8}Ba_{0.2}CoO_{3-\delta}$ lattice [9]. Similar effect would exist in $La_{0.6}Sr_{0.4}Co_{0.8}Bi_{0.2}O_{2.80}$. With the expansion of the lattices, there should be weakening of the Co–O and Bi–O bonds, and the result is the enhancement in lattice oxygen mobility. Compared to that in $La_{0.8}Ba_{0.2}Co_{0.8}Bi_{0.2}O_{2.87}$, the amount ($\delta$) of oxygen nonstoichiometry in $La_{0.6}Sr_{0.4}Co_{0.8}Bi_{0.2}O_{2.80}$ was larger because with more $Sr^{2+}$ substitution for La, more oxygen vacancies were generated. By means of controlled annealing under oxygen of high pressures between 800 and 1000 °C, Fierro and co-workers [21] synthesized a series of $LaCuO_{3-\delta}$ with various oxygen deficiencies. They found that above 450 °C, CO oxidation activity increases in the order of $La_2CuO_4$ ($\delta = 0$) <$LaCuO_{2.95}$ ($\delta = 0.05$) <$LaCuO_{2.73}$ ($\delta = 0.27$) <$LaCuO_{2.65}$ ($\delta = 0.35$) <$LaCuO_{2.55}$ ($\delta = 0.45$); the content of $Cu^{3+}$ ions is 0, 90, 46, 30, and 10%, respectively. It is apparent that $Cu^{2+}/Cu^{3+}$ ion couples play only a minor role in CO oxidation and the activity is largely controlled by the amount of oxygen nonstoichiometry in the $LaCuO_{3-\delta}$ catalysts. In the $La_{1-x}A'_xCo_{1-y}Bi_yO_{3-\delta}$ ($A'_x = Ba_{0.2}$, $Sr_{0.4}$; $y = 0, 0.2$) catalysts, the value of $\delta$ decreased in the sequence of $La_{0.6}Sr_{0.4}Co_{0.8}Bi_{0.2}O_{2.80}$ ($\delta = 0.20$) >$La_{0.8}Ba_{0.2}Co_{0.8}Bi_{0.2}O_{2.87}$ ($\delta = 0.13$) >$La_{0.6}Sr_{0.4}CoO_{2.89}$ ($\delta = 0.11$) >$La_{0.8}Ba_{0.2}CoO_{2.94}$ ($\delta = 0.06$), coinciding with the sequence of decrease in CO oxidation activity ($T_{100\%}$) as shown in Table 1. It is in agreement with Fierro and coworkers' conclusions [21]. The distribution of oxidation states of the B-site ion in $ABO_{3-\delta}$ determines the oxygen nonstoichiometry and vice versa. Actually, the $B^{n+}/B^{m+}$ ion couples influence the catalytic performance of $ABO_{3-\delta}$ indirectly via the regulation of nonstoichiometric oxygen amount and then via that of lattice oxygen mobility. The enhancement in lattice oxygen mobility (as depicted in the results of TPR, $^{18}O/^{16}O$ isotopic exchange, and CO-pulsing studies) and the presence of oxygen vacancies rendered the nonstoichiometric perovskite materials catalytically active for CO oxidation.

In the steady-state oxidation of CO over supported metal catalysts, there is a critical $CO/O_2$ molar ratio at which the rate-determining step shifts from CO adsorption to $O_2$ dissociation [22–27]. Below this critical ratio, the amount of adsorbed oxygen is higher than that of adsorbed CO; at high CO concentrations, the surface would be lack of adsorbed oxygen. Over perovskite catalysts, $O_2$ could be activated readily at structural defects. Compared to $O_2$ activation, the activation of CO over perovskites is difficult. Working on a $LaCoO_{3-\delta}$ catalyst by means of FT-IR, Tejuca and co-workers [28–30] concluded that CO adsorbs either on the oxygen atoms adjacent to Co atoms, forming carbonate species or on the Co atoms adjacent to oxygen vacancy, producing carbonyl species. Earlier, we detected both carbonyl and carbonate species after CO adsorption on $La_{0.6}Sr_{0.4}Co_{1-y}M_yO_3$ [31]. Similar species are expected to be detected on $La_{0.8}Ba_{0.2}Co_{0.8}Bi_{0.2}O_{2.87}$ and $La_{0.6}Sr_{0.4}Co_{0.8}Bi_{0.2}O_{2.80}$. The decrease in surface oxygen concentration undermines the process of lattice oxygen replenishment. As shown in Fig. 3, the $T_{100\%}$ for CO oxidation increased with the drop in $O_2$ content. One can

envision that in an $O_2$-rich atmosphere, CO oxidation could proceed at a relative lower temperature. Unlike those observed over precious metal catalysts, the catalytic activities of perovskites for CO oxidation are more sensitive to the change in space velocity. In an $O_2$-rich atmosphere (CO/$O_2$ molar ratio = 0.67/1.00), $T_{100\%}$ went up with the rise in SV (Fig. 4). Apparently, the $La_{0.8}Ba_{0.2}Co_{0.8}Bi_{0.2}O_{2.87}$ and $La_{0.6}Sr_{0.4}Co_{0.8}Bi_{0.2}O_{2.80}$ catalysts showed good performance for CO oxidation under oxidizing conditions.

It is generally believed that CO oxidation proceeds via the interaction of adsorbed CO with adsorbed [32,33] and lattice oxygen [34–38]. The former is oxygen adsorbed molecularly and dissociatively ($O_2^-$, $O^-$ or $O_2^{2-}$) at oxygen vacancies, the latter is related to the partial reduction of B-site cation [39–42]. It has been reported that the redox reactions of cobalt ions with lattice oxygen in $La_{1-x}A'_xBO_{3-\delta}$ (A′ =Ca, Sr; B = Mn, Fe, Co; $x$ = 0–1) have an important role to play in enhancing ammoxidation activity [43]. After investigating the reactivity of lattice oxygen and the desorption of oxygen over cobaltate perovskites, Nakamura et al. [44] pointed out that in the oxidation of CO, there is the involvement of lattice oxygen accompanied by the reduction of $Co^{4+}$ to $Co^{3+}$, and the formation of oxygen vacancies. Naturally, with the generation of surface vacancies, the diffusion of lattice oxygen from the bulk to the surface would become facile and the surface oxygen consumed in the reaction could be replenished. Therefore, both kinds of oxygen species are involved in the total oxidation of CO. We suggest that the catalytic activities of $La_{1-x}A'_xCo_{1-y}Bi_yO_{3-\delta}$ ($A'_x$ = $Ba_{0.2}$, $Sr_{0.4}$; $y$ = 0, 0.2) and $La_{1-x}Sr_xMO_{3-\delta}$ (in addition to the contribution of Pd) could be attributed to the extent of the redox processes of $O^2 \Leftrightarrow O_2^- \Leftrightarrow O_2^{2-} \Leftrightarrow O^- \Leftrightarrow O^{2-}_{\text{lattice}}$ lattice, $(Co^{4+}) \Leftrightarrow Co^{3+} \Leftrightarrow Co^{2+} \Leftrightarrow Co^0$, and/or $Bi^{5+} \Leftrightarrow Bi^{3+} \Leftrightarrow Bi^0$. It can be observed that among the $La_{1-x}A'_xCo_{1-y}Bi_yO_{3-\delta}$ catalysts, the more the oxygen vacancy density, the higher is the CO oxidation activity (Table 1 and Figs. 3 and 4). As illustrated in the TPR studies (Fig. 8a–d), the reduction temperature increased in the order of $La_{0.6}Sr_{0.4}Co_{0.8}Bi_{0.2}O_{2.80}$ (376 °C) <$La_{0.8}Ba_{0.2}Co_{0.8}Bi_{0.2}O_{2.87}$ (400 °C) <$La_{0.6}Sr_{0.4}CoO_{2.89}$ (440 °C) <$La_{0.8}Ba_{0.2}CoO_{2.94}$ (490 °C), coinciding with the order of decrease in $H_2$ consumption: $La_{0.6}Sr_{0.4}Co_{0.8}Bi_{0.2}O_{2.80}$ (4.81 mmol $H_2$ $g_{\text{cat}}^{-1}$) >$La_{0.8}Ba_{0.2}Co_{0.8}Bi_{0.2}O_{2.87}$ (3.12 mmol $H_2$ $g_{\text{cat}}^{-1}$) >$La_{0.6}Sr_{0.4}CoO_{2.89}$ (2.38 mmol $H_2$ $g_{\text{cat}}^{-1}$) >$La_{0.8}Ba_{0.2}CoO_{2.94}$ (1.88 mmol $H_2$ $g_{\text{cat}}^{-1}$). It means that the incorporation of $Bi^{5+}$ into the $La_{0.8}Ba_{0.2}CoO_{3-\delta}$ and $La_{0.6}Sr_{0.4}CoO_{3-\delta}$ lattices promoted the mobility of lattice oxygen. This is confirmed by the results of $^{18}O/^{16}O$ exchange (Fig. 6) and CO-pulsing (Fig. 7) studies. Generally speaking, the isotopic exchange involves six different steps as described in [45]. Since the catalyst had been purged with helium at 700 °C for 0.5 h before the pulsing of $^{18}O_2$ (this treatment would guarantee the desorption of the adsorbed oxygen species), one can preclude the existence of adsorbed $^{16}O$ species on the surface or at the oxygen vacancies of the catalyst; i.e., the $^{16}O$ atoms in the desorbed $^{18}O^{16}O$ and $^{16}O_2$ were entirely originated from the lattice of the catalyst. By comparing the relative concentrations of $^{18}O_2$, $^{18}O^{16}O$, and $^{16}O_2$, one can deduce that $^{18}O$ is readily infiltrated into the perovskite lattices of the Bi-doped cobaltate catalysts and any consumed amount of lattice oxygen is rapidly replenished above 300 °C. This oxygen redox cycle demonstrates the high mobility of lattice oxygen in $La_{0.8}Ba_{0.2}Co_{0.8}Bi_{0.2}O_{2.87}$ and $La_{0.6}Sr_{0.4}Co_{0.8}Bi_{0.2}O_{2.80}$. As shown in Fig. 7, the high $C^{18}O^{16}O$ selectivity in the range of 150–250 °C and the high CO conversion in the range of 250–450 °C reflect the high reactivity of lattice $^{18}O^{2-}$ (incorporated into in the catalysts during $^{18}O_2$ pulsing) with CO; i.e., the lattice oxygen is reactive toward CO. Therefore, the enhanced catalytic activities of $La_{0.8}Ba_{0.2}Co_{0.8}Bi_{0.2}O_{2.87}$ and $La_{0.6}Sr_{0.4}Co_{0.8}Bi_{0.2}O_{2.80}$ could be associated with the promotion in lattice oxygen mobility. It should be noted that the near 100% carbon balance at or below 450 °C precludes the possibility of CO disproportionation ($2CO \rightarrow C + CO_2$). Previously, we have reported that CO disproportionation occurred only above 460 °C over a Ni-$La_2O_3$/5A catalyst [46]. This Ni-based catalyst is expected to catalyze CO disproportionation reaction more readily than perovskite-type oxide catalysts such as $La_{0.8}Ba_{0.2}Co_{0.8}Bi_{0.2}O_{2.87}$ and $La_{0.6}Sr_{0.4}Co_{0.8}Bi_{0.2}O_{2.80}$ because metallic nickel can activate CO molecules more effectively than the base metal oxides. Based on these results and the above consideration, we conclude that the adsorbed oxygen species at oxygen vacancies and lattice oxygen species on/in the Bi-incorporated perovskite-type oxide catalysts are responsible for the low-temperature catalytic reaction of CO oxidation.

### 4.2. Structural defect, redox ion couple, and catalytic activity in $NO_x$ removal

Among the $La_{1-x}Sr_xMO_{3-\delta}$ ($x$ = 0, 0.2, 0.4) catalysts, $La_{0.8}Sr_{0.2}MO_{2.90}$ showed the best catalytic performance in the elimination of NO, giving 97% NO conversion at 260 °C for $\lambda$ = 1.00. With an increase in reaction temperature, NO conversion decreased because more CO was oxidized at high temperatures. Under oxidizing atmospheres (e.g. $\lambda$ = 1.41), the maximum NO conversion dropped from 97 to 70%; under reducing atmospheres (e.g. $\lambda$ = 0.83), however, there was an enhancement in NO conversion. Under reaction conditions similar to those adopted in the present work, $La_{0.8}Sr_{0.2}MO_{2.90}$ is superior in NO removal to $LaMn_{0.976}Rh_{0.024}O_{3.15}$ (80% NO conversion at 290 °C) as reported by Guihaume and Primet [47]. In addition to the contributions of CO and $C_3H_6$ to the good activity of NO removal over $La_{0.8}Sr_{0.2}MO_{2.90}$, NO decomposition was also a major factor for NO elimination, as demonstrated in the investigation of $NO^-$, $(NO + CO)^-$, and $(NO + C_3H_6)$-pulsing studies [10].

Depending upon the $x$ value, the $La_{1-x}Sr_xCoO_{3-\delta}$ perovskite contains certain amounts of oxygen vacancies and

$Co^{n+}$ ($n = 3, 4$) ions. When bismuth incorporated into the B-site of the $La_{1-x}Sr_xCoO_{3-\delta}$ lattice existed in pentavalency, the $\delta$ value changed from negative to positive as the extent of Sr substitution increased. At $x = 0$, the incorporation of $Bi^{5+}$ in the lattice of $La_{1-x}Sr_xMO_{3-\delta}$ caused (i) the production of interstitial oxygen (over-stoichiometric oxygen) ions, and (ii) the lattice distortion of the perovskite due to the fact that $Bi^{5+}$ is larger than $Co^{3+}$ (0.55 Å) in size. The interstitial oxygen preferred to dwell between adjacent LaO layers. Due to the presence of interstitial oxygen, the two most nearby oxygen ions in the LaO plane above the interstitial defect are repelled slightly and shifted away from their normal lattice sites [48]. Vogel et al. observed that the interstitial oxygen in $LaMnO_{3.13}$ can be removed below 500 °C by $H_2$ [49]. The gradual substitution of divalent $Sr^{2+}$ for trivalent $La^{3+}$ would subsequently neutralize the effect induced by the incorporation of $Bi^{5+}$ into the B-sites, causing the amount of interstitial oxygen to decrease and disappear ultimately. Therefore, it is reasonable to assign the two partially overlapping TPR peaks in the range of 220–360 °C observed over $LaMO_{3.07}$ (Fig. 8e) to the reduction of interstitial oxygen and/or the reduction of $Bi^{5+}$ to $Bi^{3+}$ and $Co^{3+}$ to $Co^{2+}$, and those in the range of 300–560 °C observed over $La_{0.8}Sr_{0.2}MO_{2.90}$ (Fig. 8f) and $La_{0.6}Sr_{0.4}MO_{2.81}$ (Fig. 8g) to the reduction of adsorbed oxygen and the reduction of $Bi^{5+} \rightarrow Bi^{3+} \rightarrow Bi^0$ and $Co^{3+} \rightarrow Co^{2+} \rightarrow Co^0$. As revealed in the XPS (X-ray photoelectron spectroscopy) studies [10], there was $Co^{2+}$ in $La_{1-x}Sr_xMO_{3-\delta}$ and the $Co^{2+}$ amount reduced as the $x$ value increased. During the preparation process of the $La_{1-x}Sr_xMO_{3-\delta}$ catalysts, $Co^{2+}$ and $Bi^{5+}$ ions were formed via the reaction of $Co^{3+} + Bi^{3+} \rightarrow Co^{2+} + Bi^{5+}$. Factors such as (i) lattice deformation, (ii) the existence of interstitial oxygen, and (iii) $O^{2-}$ shift in LaO planes would result in a rise in lattice oxygen mobility. An increase in lattice oxygen mobility is favorable for the catalytic elimination of NO. Besides the mobility of lattice oxygen, the concentration of oxygen vacancies is another influencing factor for NO removal. Indeed, oxygen vacancies are directly connected with lattice oxygen mobility in $La_{1-x}Sr_xBO_{3-\delta}$: the higher the number of oxygen defects (i.e. the higher the x value), the higher is the mobility of lattice oxygen [50]. It is clear that $Sr^{2+}$ substitution in A-sites increases the concentration of oxygen vacancies whereas $Bi^{5+}$ substitution in B-sites induces the presence of interstitial oxygen. Both effects result in an enhancement in lattice oxygen mobility, as revealed in $H_2$ consumption in the TPR experiments. For $La_{0.8}Sr_{0.2}MO_{2.90}$, there were the highest mobile lattice oxygen (shown in the TPR results) as well as certain amounts of oxygen vacancies in the catalyst. Hence, it is reasonable for $La_{0.8}Sr_{0.2}MO_{2.90}$ to exhibit the best catalytic performance for NO removal.

In $La_{1.867}Th_{0.100}CuO_{4-\delta}$, there were small amounts of cation defects ($\phi = 0.033$) and excess oxygen ($\delta = -0.005$) as well as $Cu^{2+}$ and $Cu^{3+}$ ions; i.e. the formula can be expressed as $La_{1.867}Th_{0.100}\phi_{0.033}CuO_{4.005}$. After reduction in $H_2$ at 300 °C, it changed into $La_{1.867}Th_{0.100}\phi_{0.033}CuO_{3.973}$ possessing cation/anion dual defects and $Cu^+/Cu^{2+}$ couple, rendering the lattice oxygen mobile in this material [11]. NO adsorbed on the surfaces of the fresh and 300 °C-reduced catalysts to form NO radicals but an intermediate $[O_2NO_2]^{2-}$ was generated via the interaction of NO with $O_2^-$ at oxygen vacancies only over the reduced sample [11], and $Cu^+$ was concomitantly oxidized to $Cu^{2+}$. Hence, the decomposition process of NO is related to a redox action between $Cu^+$ and $Cu^{2+}$ in the pre-reduced catalyst. As shown in Fig. 10, the catalytic performance of the 300 °C-reduced perovskite-like oxide was much superior to that of the fresh one; 91% NO conversion (to $N_2$) at 650 °C over the 300 °C-reduced $La_{1.867}Th_{0.100}\phi_{0.033}CuO_{3.973}$ catalyst was higher than those over Rh/γ-$Al_2O_3$ (32% at 600 °C), Pt/γ-$Al_2O_3$ (83% at 800 °C), and Cu-MFI-143 (80% at 527 °C) [51,52]. It is generally accepted that the decomposition of NO involves the dissociation of NO to nitrogen and oxygen on the catalyst surface; nitrogen readily desorbs as $N_2$ whereas the oxygen that retained on the surface deactivates the catalyst. Therefore, the desorption of the strongly attached oxygen is the rate-limiting step of the overall reactions. At high temperatures, oxygen desorption can result in the regeneration of active sites and thus enables the catalytic cycle of NO decomposition [53]. It has been reported that an "extra-lattice-oxygen (ELO) species" is involved in NO decomposition [54,55]. The ELO could exist in the form of $Cu^{2+}O_2^-$ or $Cu^{2+}O^-$ [56]. Over the 300 °C-reduced $La_{1.867}Th_{0.100}\phi_{0.033}CuO_{3.973}$ catalyst, oxygen vacancies are able to stabilize $O_2^-$ species, and the high mobility of lattice oxygen ($O^{2-}{}_{lattice}$) favors the decomposition of $[O_2NO_2]^{2-}$ that further contributes to the availability of $O^{2-}{}_{lattice}$. We believe that the redox action between $O_2^-$ and $O^{2-}{}_{lattice}$ is involved in the decomposition of NO and the enhanced DeNO activity of the reduced catalyst is due to the presence of oxygen vacancies and $Cu^+/Cu^{2+}$ couple.

In order to maintain electroneutrality, the substitution of $Nd^{3+}$ with $Ba^{2+}$ would result in the formation of oxygen vacancies or the oxidation of $Cu^{2+}$ to $Cu^{3+}$, whereas the substitution of $Nd^{3+}$ with $Ce^{4+}$ would lead to the presence of extra oxygen or the reduction of $Cu^{2+}$ to $Cu^+$. The extra oxygen exists in the form of $O^-$ (or $O_2^{2-}$) as shown in $La_2(Cu^{2+}{}_{1-x}Cu^{3+}{}_x)O_4^{2-}$ $(O^-)_\delta$ [57], in which a redox cycle between $Cu^{2+}/Cu^{3+}$ and $O^{2-}/O^-$ couples can take place [58,59]. Earlier, by using the XPS and EPR (electron paramagnetic resonance) techniques, we detected $O_2^-$ and $O^-$ (or $O_2^{2-}$) species on the 800 °C-treated (to some extent, this treatment is equivalent to partial reduction) $Nd_{1.6}Ba_{0.4}CuO_{4-\delta}$ and $Nd_{1.8}Ce_{0.2}CuO_{4-\delta}$ samples, but no significant $O^-$ signal was detected on the thermally treated $Nd_2CuO_{4-\delta}$ sample; after $N_2O$ decomposition, there were $Cu^+$, $Cu^{2+}$, and $Cu^{3+}$ ions, and $O_2^-$, $O^-$ or $O_2^{2-}$ ions on all of the three catalysts [12]. The redistribution of copper ions in different oxidation states after $N_2O$ decomposition was accompanied by the generation of oxygen vacancies and the regulation of the concentrations of the various oxygen species in/on the catalysts. In other words,

$N_2O$ decomposition involves redox actions $Cu^+ \Leftrightarrow Cu^{3+}$ and $O^{2-} \Leftrightarrow O^- (\text{or } O_2^{2-}) \Leftrightarrow O_2^- \Leftrightarrow O_2$. As shown in Table 2, after treatment in helium at 800 °C, there was a significant increase in reaction rate at 600 °C over the $Nd_2CuO_{4-\delta}$, $Nd_{1.6}Ba_{0.4}CuO_{4-\delta}$, and $Nd_{1.8}Ce_{0.2}CuO_{4-\delta}$ catalysts; the Ce- and Ba-doped catalysts performed much better than the undoped one. $N_2O$ can readily adsorb at oxygen vacancies and react with $O_2^{2-}$, $O^-$ or $O_2^-$ to form a crucial intermediate $N_2O_2^{2-}$ that decomposes into $N_2$ and $O_2$ (or into NO), leaving an oxygen vacancy and inducing the reduction of $Cu^{3+}$ to $Cu^{2+}$ and/or $Cu^{2+}$ to $Cu^+$. Hence, it is understandable that $Cu^+$, $Cu^{2+}$, and $Cu^{3+}$ ions coexist in the catalysts after $N_2O$ reaction. Below 400 °C, the catalytic activity of $Nd_{1.8}Ce_{0.2}CuO_{4.05}$ is higher than that of $Nd_{1.6}Ba_{0.4}CuO_{3.96}$. We speculate that in spite of the absence of oxygen vacancies in $Nd_{1.8}Ce_{0.2}CuO_{4.05}$, the existence of active oxygen (extra oxygen) makes the generation of $N_2O_2^{2-}$ possible. In $Nd_{1.6}Ba_{0.4}CuO_{3.96}$, although there are oxygen vacancies but due to the absence of extra oxygen, the formation of $N_2O_2^{2-}$ is difficult. As a result, the activity of $Nd_{1.6}Ba_{0.4}CuO_{3.96}$ is lower than that of $Nd_{1.8}Ce_{0.2}CuO_{4.05}$. Above 400 °C, the lattice oxygen in $Nd_{1.6}Ba_{0.4}CuO_{3.96}$ gradually becomes involved and the adsorption of $N_2O$ and the formation of $N_2O_2^{2-}$ are possible; as a result, the catalytic activity of $Nd_{1.6}Ba_{0.4}CuO_{3.96}$ increases. According to the above discussion, it can be concluded oxygen nonstoichiometry, and $Cu^{2+}/Cu^{3+}$ and/or $Cu^+/Cu^{2+}$ redox couples are needed factors for good catalytic performance in $N_2O$ decomposition. In other words, there are strong correlations between structural defect and catalytic activity, and between $Cu^{n+}/Cu^{(n+1)+}$ ($n = 1$ and 2) redox property and catalytic activity of $Nd_{2-x}A'_xCuO_{4-\delta}$ ($A'_x = Ba_{0.4}$, $Ce_{0.2}$) for the decomposition of $N_2O$.

As shown in Table 2, the fresh $YBa_2Cu_3O_7$ catalyst is of single phase and orthorhombic in structure, whereas after reduction in $H_2$ at 250 °C it transformed to a tetragonal structure with a composition close to that of $YBa_2Cu_3O_6$. With the removal of oxygen through $H_2$-reduction at 250 °C or thermal treatment at 800 °C, oxygen vacancies and trapped electrons as well as $Cu^+$ were generated in the catalyst, leading to the detection of NO-$Cu^+$ species [13]. Due to the presence of $Cu^+$ and $Cu^{2+}$ in $YBa_2Cu_3O_{6+x}$ [60] and $Cu^{2+}$ and $Cu^{3+}$ in $YBa_2Cu_3O_{7-\delta}$ [61–63], the amount of oxygen vacancies in the former sample ($x = 0.325$, i.e. $\delta = 0.675$) is larger than those in the latter one ($\delta = 0.28$) as shown in Table 2. On the fresh sample, $N_2O$ adsorption may proceed via the redox action amidst $Cu^{2+\delta} \Leftrightarrow Cu^{2+} \Leftrightarrow Cu^{2-\delta}$; on the reduced sample, $N_2O$ adsorption may proceed via the redox action amidst $Cu^{1+\delta} \Leftrightarrow Cu^+ \Leftrightarrow Cu^{1-\delta}$. During the above redox processes of copper ions, concomitant oxygen redox cycles take place: $O^{2-} \Leftrightarrow O_2^{2-} (\text{or } O^-) \Leftrightarrow O_2^- \Leftrightarrow O_2$. Considering that (i) the concentrations of oxygen vacancies, $Cu^+$ ions, trapped electrons in the reduced catalyst are larger than those in the fresh one and (ii) the conversion of $N_2O$ over the reduced catalyst was higher than that over the fresh one (Fig. 12), we conclude that $Cu^+/Cu^{2+}$ couple and trapped electrons at oxygen vacancies are active centers for $N_2O$ decomposition.

## 5. Conclusions

$La_{1-x}A'_xCo_{1-y}Bi_yO_{3-\delta}$ ($A'_x = Ba_{0.2}$, $Sr_{0.4}$; $y = 0$, 0.2) were single phase and cubic in structure whereas $La_{1-x}Sr_xMO_{3-\delta}$ ($M = Co_{0.77}Bi_{0.20}Pd_{0.03}$, $x = 0$, 0.2, 0.4) were of monophasic orthorhombic structure; there were $Co^{4+}/Co^{3+}$ ion couple in the Bi-free catalysts and $Co^{2+}/Co^{3+}$ and $Bi^{5+}/Bi^{3+}$ ion couples in the Bi-doped catalysts. The Bi-incorporated catalysts performed much better than the corresponding Bi-free catalysts and the Sr-substitution catalysts outperformed the corresponding Ba-substitution catalysts for CO oxidation. Oxygen isotope exchange experiments demonstrated that the mobility of lattice oxygen in the Bi-doped samples was much higher than that in the Bi-free samples. The results of TPR investigation showed that compared to the Bi-free catalysts, the reduction of lattice oxygen over the Bi-coped samples occurred at lower temperatures. Among the $La_{1-x}Sr_xMO_{3-\delta}$ catalysts, $La_{0.8}Sr_{0.2}MO_{2.90}$ exhibited the best catalytic activity in the oxidation of CO. The enhanced catalytic performance due to the Sr (or Ba)- and Bi-doping can be related to the concentration of oxygen vacancy and the properties of redox $Co^{n+}/Co^{(n+1)+}$ ($n = 2$, 3) and $Bi^{3+}/Bi^{5+}$ couples as well as the mobility of lattice oxygen.

In tetragonal (T structure) $La_{1.867}Th_{0.100}CuO_{4-\delta}$, there are cation defects and $Cu^{2+}/Cu^{3+}$ couple; pre-reduction at 300 °C of the sample resulted in the generation of oxygen vacancies and $Cu^+/Cu^{2+}$ couple. The pre-reduced sample showed DeNO activity higher than that of the fresh one. The redox action between $Cu^+$ and $Cu^{2+}$ is an essential process for NO decomposition. For tetragonal (T′ structure) $Nd_2{}^-{}_xA'_xCuO_{4-\delta}$ ($A'_x = Ba_{0.4}$, $Ce_{0.2}$), there are $Cu^{2+}/Cu^{3+}$ couple and oxygen vacancies in $Nd_{1.6}Ba_{0.4}CuO_{3.96}$, and $Cu^+/Cu^{2+}$ couple and over-stoichiometric oxygen in $Nd_{1.8}Ce_{0.2}CuO_{4.05}$. The $Cu^{2+}/Cu^{3+}$ and $Cu^+/Cu^{2+}$ redox couples are involved in the $N_2O$ decomposition processes. Oxygen vacancies are favorable to $N_2O$ adsorption, generating the crucial $N_2O_2^{2-}$ intermediate species. $N_2O$ decomposition activity over Ce- or Ba-doped catalyst is much better than that over the undoped catalyst ($Nd_2CuO_{4-\delta}$). This behavior is intimately related to the oxygen nonstoichiometry and copper ion redox properties. Pre-reduction is also necessary for good catalytic performance in the case of the orthorhombic $YBa_2Cu_3O_{7-\delta}$ system. The fresh sample (containing $Cu^{2+}/Cu^{3+}$ ions and less amount of oxygen vacancies) showed $N_2O$ decomposition activity lower than that of the 250 °C-reduced sample (containing $Cu^+/Cu^{2+}$ ions and more amount of oxygen vacancies). The redox action amongst $Cu^{2+\delta} \Leftrightarrow Cu^{2+} \Leftrightarrow Cu^{2-\delta}$ in the former sample and that amongst $Cu^{1+\delta} \Leftrightarrow Cu^+ \Leftrightarrow Cu^{1-\delta}$ in the latter sample are essential for $N_2O$ decomposition. The presence of oxygen vacancies

is also considered to be beneficial for the adsorption of $N_2O$.

Based on the above results, it is concluded that there is a relationship either between the structural defect (mainly oxygen vacancies) and catalytic activity or between the redox (mainly transition metal ion couples) ability and catalytic performance of these materials for CO oxidation and $DeNO_x$ processes. The generation of oxygen vacancies by A-site replacements favors the activation of $O_2$ and $NO_x$; the modification of B-site ion oxidation states by aliovalent ion substitutions in A- and/or B-sites promotes the redox process of the catalyst. The overall effect of such cationic substitutions results in a kind of catalytic materials that perform well in the elimination of CO and $NO_x$.

## Acknowledgements

The work described in this paper was fully supported by a foundation from The Education Committee of Beijing (Km200310005001) and by grants from the Hong Kong Baptist University (FRG/00-01/I-15 and FRG/97-98/I-30).

## References

[1] R.J.H. Voorhoeve, in: J.J. Burton, R.L. Gaten (Eds.), Advanced Materials in Catalysis, Academic Press, New York, 1977, p. 129.
[2] L.G. Tejuca, J.L.G. Fierro (Eds.), Properties and Applications of Perovskite-Type Oxides, Dekker, New York, 1993.
[3] W.I.F. David, W.T.A. Harris, J.M.F. Gunn, O. Moze, A.K. Soper, P. Day, J.D. Jorgensen, D.G. Hinks, M.A. Beno, L. Soderholm, D.W. Capone II, I.K. Schuller, C.U. Segre, K. Zhang, J.D. Grace, Nature 327 (1987) 310.
[4] M.F. Garbauskas, R.H. Arendt, J.S. Kasper, Inorg. Chem. 26 (1987) 3191.
[5] F. Beech, S. Miraglia, A. Santoro, R.S. Roth, Phys. Rev. B 35 (1987) 8778.
[6] J.D. Jorgensen, M.A. Beno, D.G. Hinks, L. Soderholm, K.J. Volin, R.L. Hitterman, J.D. Grace, I.K. Schuller, C.U. Segre, K. Zhang, M.S. Kleefisch, Phys. Rev. B 36 (1987) 3608.
[7] G.S. Grader, P.K. Gallagher, Adv. Ceram. Mat. 2 (1987) 649.
[8] G.H. Kwei, S.W. Cheong, Z. Fisk, F.H. Garzon, J.A. Goldstone, J.D. Thompson, Phys. Rev. B 40 (1989) 9370.
[9] H.X. Dai, H. He, W. Li, Z.Z. Gao, C.T. Au, Catal. Lett. 73 (2001) 149.
[10] H. He, H.X. Dai, C.T. Au, Appl. Catal. B 33 (2001) 65.
[11] L.Z. Gao, C.T. Au, Catal. Lett. 65 (2000) 91.
[12] L.Z. Gao, C.T. Au, J. Mol. Catal. A 168 (2001) 173.
[13] L.Z. Gao, C.T. Au, Appl. Catal. B 30 (2001) 35.
[14] H.X. Dai, C.F. Ng, C.T. Au, J. Catal. 193 (2000) 65.
[15] M. Oku, J. Kimura, M. Omori, K. Hirokawa, Fresenius Z. Anal. Chem. 335 (1989) 382.
[16] D.C. Harris, T.A. Hewston, J. Solid State Chem. 69 (1987) 182.
[17] N.R. Khasanova, A. Yamamoto, S. Tajima, X.-J. Wu, K. Tanabe, Physica C 305 (1998) 275.
[18] N.R. Khasanova, F. Izumi, T. Kamiyama, K. Yoshida, A. Yamamoto, S. Tajima, J. Solid State Chem. 144 (1999) 205.
[19] M. Zanne, C. Gleitzer, J. Aubry, J. Solid State Chem. 14 (1975) 160.
[20] Ph. Boullay, M. Hervieu, N. Nguyen, B. Raveau, J. Solid State Chem. 147 (1999) 45.
[21] H. Falcon, M.J. Martinez-Lope, J.A. Alonso, J.L.G. Fieero, Appl. Catal. B 26 (2000) 131.
[22] T. Matsushima, C.J. Musset, J.M. White, J. Catal. 41 (1976) 397.
[23] T. Matsushima, D.B. Almy, J.M. White, Surf. Sci. 67 (1977) 89.
[24] T. Matsushima, J.M. White, Surf. Sci. 67 (1977) 122.
[25] A. Golchet, J.M. White, J. Catal. 53 (1978) 266.
[26] T. Matsushima, M. Hashimoto, I. Toyoshima, J. Catal. 58 (1979) 303.
[27] M. Ehsasi, M. Matloch, D. Frank, J.H. Block, K. Christmann, F.S. Rys, W. Hirschwald, J. Chem. Phys. 91 (1989) 4949.
[28] J.M.D. Tascón, L.G. Tejuca, Z. Phys. Chem. N.F. 121 (1980) 63.
[29] J.M.D. Tascón, J.L.G. Firreo, L.G. Tejuca, Z. Phys. Chem. N.F. 124 (1981) 249.
[30] L.G. Tejuca, C.H. Rochester, J.L.G. Firreo, J. Chem. Soc., Faraday Trans. I 80 (1984) 1089.
[31] W. Li, Q. Huang, W.J. Zhang, B.X. Lin, G.L. Lu, Stud. Surf. Sci. Catal. 30 (1987) 405.
[32] Y.J. Mergler, A. van Aalst, J. van Delft, B.E. Nieuwenhuys, Appl. Catal. B 10 (1996) 245.
[33] Y.J. Mergler, J. Hoebink, B.E. Nieuwenhuys, J. Catal. 167 (1997) 305.
[34] T. Jin, T. Okuhara, G.J. Mains, J.M. White, J. Phys. Chem. 91 (1987) 3310.
[35] S.H. Oh, C.C. Eickel, J. Catal. 112 (1988) 543.
[36] G.S. Zafiris, R.J. Gorte, J. Catal. 143 (1993) 86.
[37] C. Serre, F. Garin, G. Belot, G. Maire, J. Catal. 141 (1993) 9.
[38] A.K. Tripathi, N.M. Gupta, J. Catal. 153 (1995) 208.
[39] N. Yamazoe, Y. Teraoka, T. Seiyama, Chem. Lett. (1981) 1767.
[40] C.N.R. Rao, in: C.N.R. Rao (Ed.), Chemistry of Oxide Superconductivity, Blackwell, Oxford, 1988.
[41] A. Bielañski, J. Haber, Oxygen in Catalysis, Dekker, New York, 1991.
[42] J. Haber, in: J.P. Bonnelle, B. Delmon, E. Derouane (Eds.), Surface Properties and Catalysis by Non-Metals, Reidel, Dordrecht, 1983.
[43] Y. Wu, T. Yu, B.S. Dou, C.X. Wang, X.F. Xie, Z.L. Yu, S.R. Fan, Z.R. Fan, L.C. Wang, J. Catal. 120 (1989) 88.
[44] T. Nakamura, M. Misono, Y. Yoneda, Chem. Lett. (1981) 1589.
[45] K. Klier, J. Nováková, P. Jíru, J. Catal. 2 (1963) 479.
[46] J.Z. Luo, Z.L. Yu, C.F. Ng, C.T. Au, J. Catal. 194 (2000) 198.
[47] N. Guihaume, M. Primet, J. Catal. 165 (1997) 197.
[48] M.S.D. Read, M.S. Ialam, J. Phys. Chem. B 103 (1999) 1558.
[49] E.M. Vogel, D.W. Johnson Jr., P.K. Grallagher, J. Am. Ceram. Soc. 60 (1977) 31.
[50] D. Ferri, L. Forni, Appl. Catal. B 16 (1998) 119.
[51] M. Iwamoto, H. Yahiro, K. Tanda, N. Mizuno, Y. Mine, S. Kagawa, J. Phys. Chem. 95 (1991) 3727.
[52] A. Gervasini, P. Carniti, V. Ragaini, Appl. Catal. B 22 (1999) 201.
[53] M. Iwamoto, H. Hurukawa, S. Kagawa, Stud. Surf. Sci. Catal. 28 (1986) 943.
[54] J. Valyon, W.K. Hall, J. Catal. 143 (1993) 520.
[55] J. Valyon, W.S. Millman, W.K. Hall, Catal. Lett. 24 (1994) 215.
[56] S.C. Larsen, A.W. Aylor, A.T. Bell, J.A. Reimer, J. Phys. Chem. 98 (1994) 1153.
[57] N. Casan-Pastor, P. Gomez-Romero, A. Fuetes, J.M. Navarro, M.J. Sanchis, S. Ondono, Physica C 216 (1993) 478.
[58] J.C. Grenier, A. Wattiaux, J.P. Doumerc, P. Dordor, L. Fournes, J.P. Chaminade, M. Pouchard, J. Solid State Chem. 96 (1992) 20.
[59] E. Magnone, G. Cerisola, M. Ferretti, A. Barbucci, J. Solid State Chem. 144 (1999) 8.
[60] M.S. Islam, R.C. Baetzold, Phys. Rev. B 40 (1989) 10926.
[61] J.B. Goodenough, A. Manthiram, J. Solid State Chem. 88 (1990) 115.
[62] R.C. Baetzold, Phys. Rev. B 38 (1988) 11304.
[63] G. Tavcar, B. Ogorevc, V. Hudnik, S. Pejovnik, Physica C 175 (1991) 607.